AFRL-SR-BL-TR-98-

0082

REPORT DOCUMENTATION PAG

1. AGENCY USE ONLY *(Leave Blank)*	2. REPORT DATE	3. REPORT TYPE AND DATES COVERED
	31 Dec 1997	Final Report 1 Jun 1996 — 30 Sep 1997

4. TITLE AND SUBTITLE
Simulation of Turbulent Hypersonic Flows

5. FUNDING NUMBERS
AF/F49620–96–1–0269

6. AUTHORS(S)
Graham V. Candler

7. PERFORMING ORGANIZATIION NAMES(S) AND ADDRESS(ES)
University of Minnesota
Aerospace Engineering and Mechanics
110 Union St. SE
Minneapolis, MN 55455

8. PERFORMING ORGANIZATION REPORT NUMBER

9. SPONSORING / MONITORING AGENCY NAME(S) AND ADDRESS(ES)
Air Force Office of Scientific Research
110 Bolling Avenue
Bolling AFB, DC 20332

NA

10. SPONSORING / MONITORING AGENCY REPORT NUMBER

11. SUPPLEMENTARY NOTES

12a. DISTRIBUTION / AVAILABILITY STATEMENT
Approved for public release; distribution unlimited.

12b. DISTRIBUTION CODE

13. ABSTRACT *(Maxiumum 200 words)*

Direct numerical simulations of turbulent reacting flows were performed to study the interaction between chemical heat release and turbulent fluid motion. A portion of the energy released by exothermic reactions is placed in the compressible mode of turbulent kinetic energy, with very little energy disposed to the incompressible mode. This process results in a positive feedback mechanism, whereby temperature fluctuations are amplified by the chemical reactions. In the case of endothermic reactions, the feedback is negative, resulting in decreased turbulent motion. The results of the simulations were used to develop a model for temperature fluctuations under conditions typical of a hypersonic boundary layer. This model has been validated and is suitable for use in the large–eddy simulation of hypersonic turbulent boundary layers.

14. SUBJECT TERMS	15. NUMBER OF PAGES
direct numerical simulations, turbulence, hypersonic flows	33
	16. PRICE CODE

17. SECURITY CLASSIFICATION OR REPORT	18. SECURITY CLASSIFICATION OF THIS PAGE	19. SECURITY CLASSIFICATION OF ABSTRACT	20. LIMITATION OF ABSTRACT
UNCLASSIFIED	UNCLASSIFIED	UNCLASSIFIED	UL

FINAL TECHNICAL REPORT ON:

SIMULATION OF TURBULENT HYPERSONIC FLOWS

AIR FORCE OFFICE OF SCIENTIFIC RESEARCH
Grant No. AF/F49620-96-1-0269

Graham V. Candler

Department of Aerospace Engineering and Mechanics
University of Minnesota, Minneapolis MN 55455
612-625-2364 Fax: 612-626-1558

SUMMARY

The interaction between turbulent fluid motion and finite-rate chemical reactions has not been studied under conditions typical of a high-temperature, hypersonic boundary layer. These flows are significantly different than turbulent combustion flows, which have been studied extensively. In hypersonic flows the dominant chemical reactions are the dissociation and recombination of nitrogen and oxygen molecules. These reactions are different than combustion reactions for several reasons. First, the equilibrium composition of reacting air depends strongly on the temperature. This is contrasted with a combustion process, where the equilibrium composition is determined by the initial fuel-oxidizer ratio. Another important feature of air reactions is that they have a large activation energy, and therefore the reaction rate is typically temperature limited. In this situation, the reaction rate depends exponentially on the temperature, and small increases in the temperature result in large increases in the reaction rate. This is contrasted with non-premixed combustion flows where the fuel-oxidizer mixing rate determines the rate of product formation, and the reaction process is relatively insensitive to the temperature. In premixed combustion flows, the flame speed is primarily determined by the diffusive transport of reactive radical species and heat, rather than by the reaction rate itself.

The surface of a hypersonic vehicle is typically cooled below the adiabatic wall temperature. Thus, the maximum temperature in a hypersonic boundary layer occurs some distance from the surface where there is significant shear heating and the wall cooling is not important. In this region, the air molecules dissociate, and the reaction products diffuse toward the surface where they recombine due to the cool wall. Therefore, hypersonic boundary layers, unlike combustion flows, have regions of endothermic (dissociation) reactions and exothermic (recombination) reactions.

Thus, the purpose of this project was study how turbulent temperature fluctuations interact with the finite-rate chemical reactions that occur in hypersonic boundary layers. The compressible Navier-Stokes equations, that have been extended to include the effects of finite-rate chemical reactions and heat release, are solved numerically. This allows the study of how changes in the reaction rate, heat release, and turbulent Mach number affect the decay of isotropic, homogeneous turbulence. Isotropic turbulence is the most fundamental turbulent flow, and it is a useful idealized test case. It also serves as an approximation of the small-scale turbulent motion in a boundary layer.

This report summarizes the results of the AFOSR-sponsored project, "Simulation of Turbulent Hypersonic Flows." More details of the work may be found in the two attached

papers. The first paper, "Effect of Chemical Reactions on Decaying Isotropic Turbulence," describes the results of a series of direct numerical simulations of compressible, turbulent, reacting flows that was performed as part of this project. The second paper, "Subgrid-Scale Model for the Temperature Fluctuations in Reacting Turbulence," discusses the use of the simulation data to develop a model for turbulent temperature fluctuations in hypersonic boundary layers. This model is useful for large-eddy simulations of hypersonic, turbulent boundary layers.

The research was carried out by the Principal Investigator, Graham V. Candler, and M. Pino Martin, a Graduate Research Assistant in the Aerospace Engineering and Mechanics Department at the University of Minnesota. Two conference publications resulted from this work: M.P. Martin and G.V. Candler, "Effect of Chemical Reactions on the Decay of Isotropic Homogeneous Turbulence," *AIAA Paper No. 96-2060,* June 1996; and M.P. Martin and G.V. Candler, "Evaluation of a Subgrid-Scale Model for the Temperature Fluctuations in Reacting Turbulence," *AIAA Paper No. 97-0751,* Jan. 1997. Also, this work was presented at the 1996 and 1997 American Physical Society Division of Fluid Dynamics Meetings. These two papers have been revised and submitted to *Physics of Fluids.*

KEY FINDINGS

The direct numerical simulations (DNS) of turbulent reacting flows showed that in the case of exothermic (heat-producing) reactions, a portion of the chemical energy is placed in the compressible turbulent kinetic energy modes. Almost none of this energy is placed in the incompressible turbulent kinetic energy modes. Therefore, exothermic turbulent flows tend to have a very large compressible energy component, which results in strong compressions and expansions in the flow. When the reactions are endothermic (heat-absorbing), energy is removed from the compressible energy modes.

The reacting flow that was studied was a simple perfectly mixed three-dimensional periodic box of gas that was initialized with realistic isotropic turbulence. The turbulent flow was then allowed to react and decay over time. Because this is a perfectly mixed flow, there is no turbulent length scale that is introduced into the reaction process. This causes the addition and removal of energy by exothermic and endothermic reactions to be scale-independent. This accounts for the energy affecting only the compressible energy modes.

The strength of the turbulence-chemistry interaction depends on the amount of heat

released (or absorbed) and on the rate of the reactions. Generally, the faster the reaction rate, the stronger the interaction. This shows that the chemistry-turbulence interaction depends on localization of the heat release and a self-strengthening feedback mechanism. For example, consider a region in the flow where there is a positive temperature fluctuation. If the reaction is relatively fast, the heat released by the reaction will remain in the vicinity of the original hot spot, resulting in a further increase in the temperature. However if the reaction is slow, the fluid will have moved before the heat is released and the feedback process will be weakened or eliminated.

This discussion also clarifies why the chemical energy affects the compressible kinetic energy modes. The temperature fluctuations generated by the reaction rate fluctuations produce localized regions of high and low pressure. This results in compressive and expansive (compressible or dilatational) motion of the gas.

The results are discussed in much greater detail in the attached paper, "Effect of Chemical Reactions on Decaying Isotropic Turbulence," which has been submitted to *Physics of Fluids.*

The results of the direct numerical simulations were used to formulate a model for turbulent fluctuations under conditions typical of a hypersonic cruise vehicle. This subgrid-scale model is designed for use in large-eddy simulations of these flows, and embodies the key features of the chemistry-turbulence feedback mechanism discussed above.

The subgrid-scale model represents the temperature fluctuations with a Gaussian probability density function (PDF) whose mean and variance are fitted to the DNS data over the conditions of interest. This is valid because the DNS data show that the distribution of $T'/\langle T\rangle$ (temperature fluctuation normalized by the ensemble-averaged temperature) is Gaussian. Also, the mean of this distribution is zero, which means that only the variance of the distribution must be fitted. A single parameter, λ/ℓ_E, characterizes the strength of the interaction. Here, λ is the Taylor microscale, which is a turbulent length scale; and ℓ_E is the acoustic expansion length, weighted by the non-dimensional reaction rate. For the exothermic reactions tested to date, the temperature fluctuation PDF can be characterized by a power-law fit of the form

$$\frac{T'}{\langle T\rangle} = A\left(\overline{\Delta h^\circ}\frac{\lambda}{\ell_E}\right)^B$$

where $\overline{\Delta h^\circ}$ is the non-dimensional heat release (which characterizes the strength of the reaction). A and B are fitting parameters, which depend on the Arrhenius reaction rate parameters.

If the reaction is endothermic, a simpler fit may be used, depending solely on the turbulent Mach number, independent of the reaction type.

Preliminary tests of this model for several air reactions under a wide range of conditions give good agreement with the original simulations. Again, the details of the model and the comparison of the model with the original DNS data are presented in the attached paper, "Subgrid-Scale Model for the Temperature Fluctuations in Reacting Turbulence." Therefore, this model has the potential for use in large-eddy simulations of hypersonic boundary layers.

Effect of chemical reactions on decaying isotropic turbulence

M. Pino Martín

Graham V. Candler

Department of Aerospace Engineering and Mechanics
University of Minnesota
110 Union St. SE, Minneapolis, MN 55455

candler@aem.umn.edu

There are many studies of turbulent combustion flows, however there is no analysis of the interaction between turbulent motion and the chemical reactions that typically occur in hypersonic flows. In this case, the rate of product formation depends almost exclusively on the temperature, and small temperature fluctuations may produce large increases in product formation. To study this process, we perform direct numerical simulations of isotropic turbulence decay under conditions typical of a hypersonic flow. We find a positive feedback mechanism between the turbulence and the exothermic reactions. In high temperature regions the reaction rate increases, further increasing the heat released and the temperature. Simultaneously, the heat released increases the pressure, causing localized expansions and compressions that feed the turbulent kinetic energy. The Reynolds stress budget shows that the feedback occurs through the pressure-strain term. The strength of the feedback depends on how much heat is released, the rate at which it is released, and the turbulent Mach number. The feedback is negative for endothermic reactions.

I. Introduction

The interaction between turbulent fluid motion and finite-rate chemical reactions has not been studied under conditions typical of a high-temperature, hypersonic boundary layer. These flows are significantly different than turbulent combustion flows, which have been studied extensively. In hypersonic flows the dominant chemical reactions are the dissociation and recombination of nitrogen and oxygen molecules. These reactions are different than combustion reactions for several reasons. First, the equilibrium composition of reacting air depends strongly on the temperature. This is contrasted with a combustion process, where the equilibrium composition is determined by the initial fuel-oxidizer ratio. Another important feature of air reactions is that they have a large activation energy, and therefore the reaction rate is typically temperature limited. In this situation, the reaction

rate depends exponentially on the temperature, and small increases in the temperature result in large increases in the reaction rate. This is contrasted with non-premixed combustion flows where the fuel-oxidizer mixing rate determines the rate of product formation, and the reaction process is relatively insensitive to the temperature. In premixed combustion flows, the flame speed is primarily determined by the diffusive transport of reactive radical species and heat, rather than by the reaction rate itself.[1]

The surface of a hypersonic vehicle is typically cooled below the adiabatic wall temperature. Thus, the maximum temperature in a hypersonic boundary layer occurs some distance from the surface where there is significant shear heating and the wall cooling is not important. In this region, the air molecules dissociate, and the reaction products diffuse toward the surface where they recombine due to the cool wall. Therefore, hypersonic boundary layers, unlike combustion flows, have regions of endothermic (dissociation) reactions and exothermic (recombination) reactions.

Thus, it is the purpose of this paper to study how turbulent temperature fluctuations interact with the finite-rate chemical reactions that occur in hypersonic boundary layers. We numerically solve the compressible Navier-Stokes equations that have been extended to include the effects of finite-rate chemical reactions and heat release. We study how changes in the reaction rate, heat release, and turbulent Mach number affect the decay of isotropic, homogeneous turbulence. Isotropic turbulence is the most fundamental turbulent flow, and it is a useful idealized test case. It also serves as an approximation of the small-scale turbulent motion in a boundary layer.

Many direct numerical simulations of reacting turbulent flows have been reported for combustion applications.[2–14] However, as mentioned above, these simulations focus on different issues than the current paper. For example, Gao and O'Brien[6] and Javery *et al.*[14] consider the interaction of chemical reactions with homogeneous turbulence, but the reaction rate is taken as constant and the effects of heat release are not considered. Picart *et al.*[3] consider a concentration-dependent reaction rate to simulate the exponential dependence of the reaction rate on temperature, but their simulations do not include heat release effects. Several simulations of reacting shear layers have been performed including the effects of heat release. McMurtry *et al.*[5] and Grinstein and Kailasanath[8] use a constant reaction rate, Givi *et al.*[7] and Miller *et al.*[10], consider both constant and temperature-dependent reaction rates. These simulations show a significant effect of heat release on the structure of the mixing layers studied. Therefore, the previous simulations have some similarity to those presented here, but they focus on different, combustion-related issues.

In the remainder of the paper, we introduce the equations of motion and relevant non-

dimensional parameters for a mixture of reacting gases. We then discuss the formulation of our direct numerical simulations and present the results. Finally, we analyze the chemistry-turbulence interaction process and summarize our findings.

II. Governing equations

The equations describing the unsteady motion of a reacting flow with no contribution of vibrational modes are given by the species mass, mass-averaged momentum, and total energy conservation equations

$$\frac{\partial \rho_s}{\partial t} + \frac{\partial}{\partial x_j}\Big(\rho_s u_j + \rho_s v_{sj}\Big) = w_s$$

$$\frac{\partial \rho u_i}{\partial t} + \frac{\partial}{\partial x_j}\Big(\rho u_i u_j + p\delta_{ij} - \tau_{ij}\Big) = 0 \tag{1}$$

$$\frac{\partial E}{\partial t} + \frac{\partial}{\partial x_j}\Big((E+p)u_j - u_i\tau_{ij} + q_j + \sum_s \rho_s v_{sj} h_s\Big) = 0$$

where w_s represents the rate of production of species s due to chemical reactions; ρ_s is the density of species s; u_j is the mass-averaged velocity in the j direction; v_{sj} is the diffusion velocity of species s; p is the pressure; τ_{ij} is the shear stress tensor given by a linear stress-strain relationship; q_j is the heat flux due to temperature gradients; h_s is the specific enthalpy of species s; and E is the total energy per unit volume given by

$$E = \sum_s \rho_s c_{vs} T + \tfrac{1}{2}\rho u_i u_i + \sum_s \rho_s h_s^\circ, \tag{2}$$

where c_{vs} is the specific heat at constant volume of species s; and h_s° represents the heat of formation of species s.

To derive the expression for w_s, consider a reaction where species S1 reacts to form species S2

$$\mathrm{S1} + \mathrm{M} \rightleftharpoons \mathrm{S2} + \mathrm{M}, \tag{3}$$

where M represents a collision partner, which is either S1 or S2 in this case. The source terms for S1 and S2 can be written using the law of mass action

$$\begin{aligned} w_{\mathrm{S1}} = &- M_{\mathrm{S1}} k_f \frac{\rho_{\mathrm{S1}}}{M_{\mathrm{S1}}}\Big(\frac{\rho_{\mathrm{S1}}}{M_{\mathrm{S1}}} + \frac{\rho_{\mathrm{S2}}}{M_{\mathrm{S2}}}\Big) \\ &+ M_{\mathrm{S1}} k_b \frac{\rho_{\mathrm{S2}}}{M_{\mathrm{S2}}}\Big(\frac{\rho_{\mathrm{S1}}}{M_{\mathrm{S1}}} + \frac{\rho_{\mathrm{S2}}}{M_{\mathrm{S2}}}\Big), \end{aligned} \tag{4}$$

and $w_{S2} = -w_{S1}$. k_f and k_b are the forward and backward reaction rates respectively; These are written as

$$\begin{aligned} k_f &= C_f T^{\eta} e^{-\theta/T}, \\ k_b &= \frac{k_f}{K_{eq}}, \end{aligned} \tag{5}$$

where K_{eq} is the temperature-dependent equilibrium constant.

For a two species mixture, the diffusion velocity can be accurately represented using Fick's law

$$\rho_s v_{sj} = -\rho D \frac{\partial c_s}{\partial x_j}, \tag{6}$$

where $c_s = \rho_s/\rho$ is the mass fraction, and D is the diffusion coefficient given in terms of the Lewis number

$$Le = \frac{\rho D Pr}{\mu}, \tag{7}$$

where Pr is the Prandtl number, μ is the viscosity, and Le is taken to be unity, so that the energy transport due to mass diffusion is equal to the energy transport due to thermal conduction.

III. Governing parameters

In this section, we introduce the non-dimensional numbers governing the physical process. From a non-dimensional analysis of the governing equations, the following parameters are obtained: turbulent Mach number, M_t; Reynolds number based on the lateral Taylor microscale, Re_λ; Damköhler number, Da; and relative heat release, $\overline{\Delta h^\circ}$. The turbulent state of the flow gives rise to the first two non-dimensional numbers; the second two are present if the flow is chemically reacting. These parameters may be written as

$$\begin{aligned} M_t &= \frac{q}{a}, & Re_\lambda &= \frac{\rho u' \lambda}{\mu}, \\ Da &= \frac{\lambda |w|}{\rho u'}, & \overline{\Delta h^\circ} &= -\frac{\Delta h^\circ}{c_v T + \frac{1}{2} q^2}, \end{aligned} \tag{8}$$

where q is the RMS magnitude of the fluctuation velocity; a is the speed of sound; u' is the RMS turbulent velocity fluctuation in one direction; $\Delta h^\circ = h^\circ_{S2} - h^\circ_{S1}$ is the heat of the reaction; and c_v is the mixture specific heat at constant volume.

The Damköhler number is the ratio of the turbulent time scale, τ_t, to the chemical time scale, τ_c, and represents a non-dimensional reaction rate; here $\tau_t = \lambda/u'$ and $\tau_c = \rho/|w|$. $\overline{\Delta h^\circ}$ is the ratio of the chemical energy released or absorbed to the sum of the internal and

kinetic energy. A negative value indicates an endothermic reaction, and a positive value denotes an exothermic reaction.

IV. Numerical experiments

It is the purpose of this paper to determine how turbulent motion interacts with the chemical reactions that occur in hypersonic boundary layers. A logical reaction to consider is the dissociation and recombination of nitrogen, $N_2 + M \rightleftharpoons 2N + M$. However, we have found that it is difficult to analyze the effects of this reaction on the decay of isotropic turbulence because many parameters change simultaneously during the reaction. For example, consider a case where we start with pure nitrogen atoms, and let them recombine according to the reaction rate and equilibrium constant expressions given by Gupta *et al.*[21] Figure 1 plots the nitrogen molecule mass fraction for simulations with initial temperatures between 2000 and 7000 K (corresponding to values of relative heat release between 33 and 9). We see that the equilibrium mass fraction depends on the initial temperature because the equilibrium constant is a function of temperature. More importantly, the rate of reaction differs in each simulation. The differences between the simulations make it difficult to compare the effects of turbulent motion on the evolution of the chemical reactions. Therefore, we must devise a simplified chemical model that captures the key features of air reactions, yet makes it possible to compare simulations.

There are several issues that we must consider. First, if the average molecular weight of the gas changes when the reaction occurs, then the mixture-averaged gas constant and specific heats change. Therefore, changes in the pressure and internal energy will not only be due to the heat released by the reaction, but also due to the changing properties of the gas mixture. To circumvent this issue, we let the reactant and product have the same molecular weight and the same number of internal degrees of freedom; thus the mixture gas constant and specific heats do not change as the reaction progresses. For the same reason, we use the simple binary reaction given in (3), rather than a dissociation reaction in which the average molecular weight of the gas changes as a result of the reaction.

As discussed above, the equilibrium constant is a function of temperature, which implies a different chemical equilibrium state for simulations with different heat release. Therefore, we take K_{eq} to be constant, so that the equilibrium chemical state is fixed. This allows us to systematically compare simulations with different initial conditions and values of heat release.

The reaction rate is also a function of temperature. When the gas temperature goes up the reaction rate grows exponentially, which presents similar problems with comparing one

simulation to another. Therefore, we must modify the Arrhenius form of the reaction rate given by (5). It is desirable that the modified reaction rate be constant when there are no temperature fluctuations, and that the rate vary exponentially when there are temperature fluctuations. One such reaction rate expression is given by

$$\begin{aligned}\tilde{k}_f(T) &= C\frac{e^{-\theta/T}}{e^{-\theta/\langle T\rangle}}, \\ &= C\Big(1+\frac{\theta}{\langle T\rangle}\frac{T'}{T}+\frac{1}{2}\Big(\frac{\theta}{\langle T\rangle}\frac{T'}{T}\Big)^2+\ldots\Big),\end{aligned} \tag{9}$$

where $\langle T\rangle$ is the ensemble average of the temperature, $T' = T - \langle T\rangle$ is the temperature fluctuation, C is a constant, and θ is the activation temperature given in (5). If for both reaction rate expressions, we compute the ratio of the reaction rate at temperature T, to that at the ensemble-average temperature, $\langle T\rangle$, we obtain

$$\frac{k_f(T)}{k_f(\langle T\rangle)} = \frac{\tilde{k}_f(T)}{\tilde{k}_f(\langle T\rangle)} = e^{-\left(\theta/T-\theta/\langle T\rangle\right)}. \tag{10}$$

Note that we have neglected the pre-exponential factor in the reaction rate, T^η, because for the reactions that occur in hypersonic flows, $\eta \leq -1$. Thus, at large temperatures, this factor has a weak, sub-linear variation with temperature. Therefore, the two rate expressions give the same variation of the relative reaction rate for any temperature fluctuation. The only difference is that the modified reaction rate expression gives a constant rate when the temperature is equal to the ensemble-average temperature. Thus, the modified reaction rate has the important features of the Arrhenius rate expression, yet allows us to systematically compare simulations.

V. Numerical method and initial conditions

In this section we present the numerical simulations for three-dimensional, compressible, homogeneous, isotropic, reacting turbulent flow. The numerical method used is based on the method of Lee *et al.*[15] We use a sixth-order accurate finite-difference method based on a compact Padé scheme and fourth-order accurate Runge-Kutta time integration. The simulations were performed on grids with 96^3 points following the criteria given by Reynolds[16] and a resolution of $K\eta = 1$ at the end of the simulation, where K is the maximum wavenumber resolvable on the grid and η is the Kolmogorov scale. The computational domain is a periodic box with non-dimensional length 2π in each direction. The velocity field is initialized to an isotropic state prescribed by the following energy spectrum

$$E(k) \sim k^4 \exp\left[-2\Big(\frac{k}{k_o}\Big)^2\right], \tag{11}$$

where k is the integer non-dimensional wavenumber, and k_o is the most energetic wavenumber.

As Ristorcelli and Blaisdell[17] show, in a physically consistent initialization of compressible homogeneous, isotropic turbulence, there are finite density, temperature, and dilatational fluctuations. Therefore, we use their initial conditions and have compared and validated our flow initialization with that of Blaisdell and Ristorcelli.[18]

We let the turbulence evolve to a realistic state before allowing the reaction to progress. Because the initial field is weakly compressible, we use mean values of velocity derivative skewness, S_i, to predict the onset of realistic turbulence. Experimental data presented by Tavoularis *et al.*[19] and Orszag *et al.*[20] show that S_i is in the range $[-0.6 : -0.35]$ for Re_λ near 50. With this criterion, the turbulence has developed to a realistic, isotropic state at $t/\tau_t = 0.35$. The reaction is started at this time, and we measure the evolution of the turbulence relative to this time.

We run cases with combinations of $\overline{\Delta h^\circ} = -0.5$, 1.0, 1.5, and 2.0; $Da = 0.5$, 1.0, and 2.0; $M_t = 0.173$, 0.346, and 0.519; and $Re_\lambda = 25.0$, 34.5, and 50.0. We use nitrogen atoms for both species S1 and S2, with initial mass fractions of $c_{S1} = 1$ and $c_{S2} = 0$. We choose $K_{eq} = 1$, so that the chemical equilibrium is reached when $c_{S1} = c_{S2} = 0.5$. k_o is set to 4. To simplify the comparison of different simulations, we freeze μ at its initial value, and we use $Pr = 0.72$. We specify the initial density as $\rho_o = 1.0\,\mathrm{kg/m^3}$. To be consistent with the physical N_2 dissociation rate, we use $\theta = 113,200\,\mathrm{K}$.

Having introduced the modified reaction rate (9), we must specify a initial temperature that is representative of a hypersonic boundary layer and consistent with the physically correct reaction rate (5). Using the law of mass action given by (4) and assuming that we initialize the flow with pure S1, we can obtain an expression for the initial source term and combine it with (8) to derive the initial rate of reaction

$$k_f = \frac{1}{3}\,\frac{\gamma\, M_t^2\, Da\, \hat{R}\, T_{ref}^n}{\mu_{ref}\, Re_\lambda}\, T^{1-n}, \tag{12}$$

where we have taken μ from a power law ($\mu = \mu_{ref}(T/T_{ref})^n$), μ_{ref} from a Sutherland law,[21] and $\hat{R}$ is the universal gas constant. In order to obtain realistic conditions, we choose the parameters in the modified reaction rate expression, (9), to be representative of the nitrogen dissociation reaction. To do so, we use the N_2 dissociation rate expression[21]

$$k_f = 3.71 \times 10^{21}\, T^{-1.6}\, e^{-113{,}200/T} \quad (\mathrm{cm^3/mole\ s}). \tag{13}$$

We then set this expression equal to the reaction rate in terms of the non-dimensional parameters, (12), and find the temperature that satisfies this relation. For $M_t = 0.3$,

$Da = 0.5$, $T_{ref} = 300\,\mathrm{K}$, $Re_\lambda = 50$, and $\mu_{ref} = 2.106 \times 10^{-4}\,\mathrm{kg/m\,s}$, and nitrogen ($n = 0.7722$), we obtain an initial value of $T = 9470\,\mathrm{K}$. This initial temperature is characteristic of a high-temperature hypersonic boundary layer.

VI. Results

We first focus on how the chemical reactions affect the gas dynamics, leaving the discussion of chemistry and turbulence interaction for the next section. During a typical reacting simulation, the average concentration of species S1 decreases as the average concentration of species S2 increases. It should be noted that as the chemical species reach the equilibrium mass fraction, $c_{S1} = c_{S2} = 0.5$, the rate at which energy is added to or removed from the fluid approaches zero.

A. Relative Heat Release

In this section, we illustrate the effect of variations of the relative heat release at moderate Da, M_t, and Re_λ ($Da = 1$, $M_t = 0.346$, and $Re_\lambda = 34.5$). In all cases the non-reacting simulation is shown for comparison purposes. As mentioned earlier, the relative heat release is proportional to the ratio of energy released or absorbed in the formation of product species. Therefore, an increase in $\overline{\Delta h^\circ}$ increases the energy in the flow field. This is illustrated in Fig. 2a, which plots the temporal evolution of the average temperature. Figure 2b shows the temporal evolution of the turbulent kinetic energy for the different values of $\overline{\Delta h^\circ}$. When $\overline{\Delta h^\circ} = 1$, there is an initial period of time when the turbulence is enhanced. A further increase of the heat release considerably enhances the turbulent kinetic energy, maintaining and feeding the turbulence for a longer period of time. For $\overline{\Delta h^\circ} = 2$, the turbulent kinetic energy reaches high values. However, at about $t/\tau_t = 1.3$, it decays slightly more rapidly than in the other three simulations.

Turbulent motion is dissipative, and needs a supply of energy to keep from decaying. Moyal[22] decomposed the velocity field in Fourier space, $\hat{\vec{u}}$, into the incompressible (divergence-free), $\hat{\vec{u}}^I$, and compressible (curl-free), $\hat{\vec{u}}^C$, components

$$\begin{aligned} \hat{\vec{u}}^I &= \hat{\vec{u}} - \frac{\vec{k}\cdot\hat{\vec{u}}}{k^2}\vec{k}, \\ \hat{\vec{u}}^C &= \hat{\vec{u}} - \hat{\vec{u}}^I. \end{aligned} \tag{14}$$

The dissipation for isotropic turbulence can then be written as

$$\epsilon = 8\pi\nu \int_0^\infty \Big(E^I(k) + \tfrac{4}{3}E^C(k)\Big)k^2\,\mathrm{d}k, \tag{15}$$

where E^I and E^C represent the incompressible and compressible components of the shell-averaged energy spectrum

$$E^C = \frac{\hat{\vec{u}}^C \cdot \hat{\vec{u}}^C}{2\ k}, \qquad E^I = \frac{\hat{\vec{u}}^I \cdot \hat{\vec{u}}^I}{2\ k}. \tag{16}$$

From (15) we see that as the compressibility of the flow increases, the turbulence becomes more dissipative. This explains the increased rate of turbulent kinetic energy decay for the higher heat release flows.

Figure 2c shows the evolution of the relative compressible energy ratio

$$\chi = \frac{\int E^C(k)\,\mathrm{d}k}{\int \left(E^C(k) + E^I(k)\right)\,\mathrm{d}k}. \tag{17}$$

Because the simulations begin with weakly compressible conditions, when the turbulence reaches a realistic state, the initial values of χ are very low. For the endothermic reaction, χ is very small throughout the simulation, and as $\overline{\Delta h^\circ}$ is increased, the relative compressible kinetic energy increases. For a relative heat release of $\overline{\Delta h^\circ} = 2$, χ increases rapidly and reaches about 20% of the total kinetic energy at $t/\tau_t = 1.3$. Also note that there are time-dependent oscillations in χ that increase with the heat release.

Consider the energy spectrum of the flow field decomposed into its incompressible and compressible components at several different times during the simulations. Figure 3a plots these spectra for the non-reacting simulation. We observe that the compressible modes are about two orders of magnitude less energetic than the incompressible modes at all but the smallest scales. However, note that for $k\eta > 1$, the length scales are not resolved by the simulation; thus the increase in compressible energy spectrum at large wavenumber (small scales) is due to aliasing errors. (However, the level of error is small.) As time evolves, the compressible energy spectrum decays slightly at all scales, whereas the incompressible modes decrease at the large scales, and increase at the small scales.

Figure 3b plots the energy spectra for the endothermic simulation. The compressible modes are still two orders of magnitude below the incompressible modes. As time evolves, they decrease further over all except the largest scales. Figure 3c plots the energy spectra for $\overline{\Delta h^\circ} = 2$. At all scales, the energy in the compressible modes is about two orders of magnitude higher in this case than in the non-reacting case, even surpassing the incompressible modes at the largest and smallest scales. We see that the compressible modes become more energetic as $\overline{\Delta h^\circ}$ is increased, but the incompressible modes are essentially

unaffected by the level of heat release. This is shown in Fig. 4, which plots the energy spectra at $t/\tau_t = 1.5$ for the non-reacting simulation and the case with the highest heat release. The incompressible energy spectra are nearly identical. It is also interesting to note that the compressible energy spectrum is increased by the same factor at all scales (except at small scales where the aliasing error is important). This is consistent with the argument that because reactions are inherently a molecular-scale process, they must be scale independent.[23]

In Fig. 5, we observe a large increase in the RMS magnitude of the temperature fluctuations when the heat release is increased. Recall that from (9), a positive temperature fluctuation causes an exponential increase in the reaction rate. If the reaction is exothermic, heat is released and the local temperature increases. This further increases the temperature fluctuations, and the process feeds upon itself. However, because there is turbulent motion, the heated fluid may move to a different location before the reaction progresses further, reducing or eliminating the feedback process. Thus, the interaction between the chemical heat release and the turbulent motion should depend on the amount of heat released, $\overline{\Delta h^\circ}$, and the rate at which it is released, Da. Note that as the reaction progresses toward completion, the rate of formation of the products decreases. Therefore, the net rate of heat release decreases as well, and there is less energy to drive the fluctuations, causing them to decrease in time. The opposite occurs for the endothermic case: T'_{RMS} decreases initially, and then increases in time as the turbulent kinetic energy decays.

B. Damköhler Number

The Damköhler number is the ratio of the chemical reaction rate to the rate of turbulent motion. For larger values of Da, chemical equilibrium is reached in a shorter time, which causes more rapid heat addition or removal. To illustrate the effect of the Damköhler number, we consider a case of moderate heat release, turbulent Mach number, and Reynolds number ($\overline{\Delta h^\circ} = 1$, $M_t = 0.346$, and $Re_\lambda = 34.5$). Note that the total amount of energy added to the flow is the same for all simulations.

Consider Fig. 6a, which shows the temporal evolution of the average concentration of the reactant species. We observe that as Da is increased, the reactants approach equilibrium at earlier times. Figure 6b plots the evolution of the turbulent kinetic energy. Early in the simulations, the turbulent motion is enhanced with increased Da. Accordingly, the relative compressible kinetic energy of the flow increases with increased Da. As before, the compressible energy spectrum also becomes more energetic, whereas the incompressible spectra are nearly identical for all simulations. Figure 6c illustrates that increased

Da also increases the RMS temperature fluctuations. This occurs because larger reaction rate cause the heat released to remain confined to a smaller volume of fluid, enhancing the subsequent effect on the turbulence. Thus, the localization of the heat release is important in maintaining the feedback process.

C. Turbulent Mach Number

To describe the effect of the turbulent Mach number, we choose a case of moderate Damköhler number, relative heat release, and Reynolds number ($Da = 1$, $\overline{\Delta h^\circ} = 1$, and $Re_\lambda = 34.5$). For all cases, increasing the initial Mach number causes higher values of $\langle T \rangle$ since the higher turbulent kinetic energy is dissipated and converted into internal energy. In the non-reacting simulations, the relative turbulent kinetic energy, q^2/q_o^2, decay rate depends weakly on the initial M_t. For the exothermic simulations, the turbulent kinetic energy increases initially. This increase is proportional to the initial M_t.

Figure 7 plots the temporal evolution of RMS temperature fluctuations, $T'_{\rm RMS}$, for the case with $\overline{\Delta h^\circ} = 1$. This plot shows that the level of the temperature fluctuations is proportional to M_t^2; this is also the case in the non-reacting flows. However, relative to the non-reacting flow, the heat release increases $T'_{\rm RMS}$ by about a factor of two for all M_t. Thus, the heat release amplifies the kinetic energy fluctuations, resulting in higher temperature fluctuations.

D. Reynolds Number

From the direct numerical simulations we conclude that there is very little effect on the decay of reacting turbulence due to initial Reynolds numbers over the narrow range tested ($25 \leq Re_\lambda \leq 50$). We observe no variation in the rate of reaction. At higher Reynolds numbers the dissipation rate is reduced, and therefore, the temperature increases more slowly and the RMS temperature fluctuations are somewhat larger. However, these effects are insignificant compared to the variation of the other parameters.

VII. Interaction and feedback mechanism

The effects of the parameters that govern the interaction between the turbulent motion and the chemical reactions have been described in the previous section. We find that: The magnitude of the temperature fluctuations increases dramatically with either increased exothermicity or increased rate of reaction. The incompressible energy modes are virtually unaffected by the chemical reactions, whereas the compressible modes are strongly enhanced. The levels of compressibility increase with increased exothermicity

and with increased reaction rate. From these results we can conclude that there is a feedback mechanism between the turbulent motion and the chemical reactions.

The velocity decomposition (14) is unique, and the vorticity is only a function of the incompressible velocity component. Thus, if the chemical reactions affect the incompressible component of velocity, the vorticity would also be affected. Therefore, let us consider the evolution of the vorticity during the simulations. We can write the total change of vorticity as

$$\frac{D\vec{\omega}}{Dt} = (\vec{\omega}\cdot\nabla)\vec{u} - \vec{\omega}(\nabla\cdot\vec{u}) + \nabla T\times\nabla S, \tag{18}$$

where S is the entropy and we have neglected the diffusive terms. These terms represent the production of vorticity due to vortex line stretching, compressibility, and thermodynamic changes, respectively. We can decompose the third term by noting that for a mixture of thermally perfect gases

$$S = c_p \ln T - R\ln p + \sum_s c_s \frac{h_s^\circ - \mu_s^\circ}{T}, \tag{19}$$

where c_p is the specific heat at constant pressure of the gas mixture, R is the gas constant, and μ_s° is the chemical potential of species s. The first two terms form part of the entropy even when the gas is not chemically reacting, and the third term is the entropy due to chemical reactions. Thus, we can separate the production of vorticity due to thermodynamic changes into two components, and refer to them as the non-reacting entropy and the reacting entropy. Note that had we used a more complicated reaction, it would be more difficult to make this decomposition because the mixture c_p and R would also change.

Figure 8a plots the budget of vorticity for a non-reacting simulation and an exothermic simulation with $\overline{\Delta h^\circ} = 2$. There is a large difference in the order of magnitude between the terms. The main contribution to vorticity production is due to the vortex stretching and turning term for both simulations. Whereas the compressibility term remains nearly unchanged for the non-reacting case, it reaches the same order of magnitude as the stretching term for the exothermic simulation. The thermodynamic effects due to the non-reacting entropy are larger for the exothermic simulation, although they are three orders of magnitude below the terms mentioned above. The thermodynamic contribution due to the reacting entropy is initially zero for the exothermic simulation, but increases to a value that is about an order of magnitude lower than the stretching and compressible terms. Thus, the main contributions to the vorticity budget are the vortex line stretching and turning and compressibility effects.

Figure 8b illustrates the same vorticity budget for the non-reacting simulation and an endothermic case with $\overline{\Delta h^\circ} = -1$. Again, the main contribution to vorticity production

is from the vortex line stretching and turning term. For the endothermic simulation, the compressible destruction increases and the reacting entropy production is non-zero, but small.

Figure 9 plots the temporal evolution of the average vorticity magnitude for the non-reacting case and the two previous reacting cases. We see that the vorticity increases with increasing heat release. This is consistent with the increased production mechanisms shown in Fig. 8.

Our explanation of these results is as follows. The heat released does not produce vorticity by itself. Rather, the chemical reactions affect the turbulence locally, enhancing compressions and expansions. These compression and expansion regions interact with one another and generate vorticity. Greenberg[24] deduced that due to the symmetry of the problem, the third term in (18) does not contribute appreciably to the production of vorticity. Therefore, the indirect contribution to vorticity from the chemical heat release must be in the vortex stretching and turning terms and in the production of vorticity due to compressibility. Our results agree with Greenberg's analysis.

The results also corroborate the theoretical work of Eschenroeder,[25] who found that the turbulent motion is fed from the external energy source provided by the chemical reactions. Our results show that the chemical energy produces local high temperature and pressure regions, which then produce increased kinetic energy through the reversible work term, $p\nabla \cdot \vec{u}$, in the kinetic energy equation. We can see the effect of this process on the Reynolds stress by considering the Reynolds stress budget

$$R_{ij,t} = -\left(Q_{i,j} + Q_{j,i}\right) + \nu R_{ij,kk} - T_{ijk,k} - \nu\epsilon_{ij} + \Pi_{ij}. \tag{20}$$

Where $R_{ij} = \overline{u_i u_j}$ is the Reynolds stress tensor, $Q_i = \overline{pu_i/\rho}$ is the pressure-velocity correlation, $T_{ijk} = \overline{u_i u_j u_k}$ is the triple velocity correlation tensor, $\epsilon_{ij} = 2\overline{u_{i,k}u_{j,k}}$ is the homogeneous dissipation rate tensor, and $\Pi_{ij} = \overline{p(u_{i,j} + u_{j,i})/\rho}$ is the pressure-strain term. The pressure transport and the turbulent transport are statistically zero. Figure 10 shows the budget of the $R_{22,t}$ component for the non-reacting and exothermic simulations. The pressure-strain term is nearly zero in the non-reacting case, but it is the dominant term in the exothermic simulation. Note that in this case, there are oscillations in the pressure-strain production term, whose normalized period is approximately equal to the local Mach number. This indicates that these oscillations are a result of acoustic (pressure) waves. This further illustrates that the Reynolds stress generation is mainly caused by compressibility effects in the reacting case.

VIII. Conclusion

In this paper we investigated the interaction of isotropic turbulence and a chemical reaction at conditions typical of a hypersonic boundary layer. We used a modified reaction rate that preserves the important features of the Arrhenius rate expression, and makes it possible to perform a systematic analysis. The flow is parameterized by four non-dimensional numbers: the turbulent Mach number, Reynolds number, relative heat release, and relative reaction rate.

The direct numerical simulations show that the heat released by an exothermic reaction produces regions of high temperature and pressure. This causes localized expansions which increase the compressible turbulent kinetic energy. This results in increased rates of kinetic energy decay, vorticity production, and Reynolds stress production. Simultaneously, in regions of high temperature the reaction rate increases, further increasing the heat release and the temperature. Thus, there is a positive feedback between the chemical reaction and the turbulent motion. The strength of the feedback process depends on the amount of heat released, the reaction rate, and more weakly on the turbulent Mach number. When the reaction is endothermic, the feedback is negative and temperature fluctuations are damped.

We would like to acknowledge support from the Air Force Office of Scientific Research Grant number AF/F49620-96-1-0269. This work was also sponsored by the Army High Performance Computing Research Center under the auspices of the Department of the Army, Army Research Laboratory cooperative agreement number DAAH04-95-2-0003 / contract number DAAH04-95-C-0008, the content of which does not necessarily reflect the position or the policy of the government, and no official endorsement should be inferred. A portion of the computer time was provided by the University of Minnesota Supercomputing Institute.

References

[1] I. Glassman, *Combustion,* 3rd Ed., Chap. 4, Academic Press, (1996).

[2] A.D. Leonard, and J.C.Hill, "Direct numerical simulation of turbulent flows with chemical reaction," J. Sci. Comput. **3**, 25 (1988).

[3] A. Picart, R. Borghi, and J.P. Chollet, "Numerical simulation of turbulent reactive flows," Computers & Fluids **16**, 475 (1988).

[4] W.H. Jou, and J.J. Riley, "Progress in direct numerical simulations of turbulent reacting

flows," AIAA J. **27**, 1543 (1989).

[5]P.A. McMurtry, J.J. Riley, and R.W. Metcalfe, "Effects of heat release on the large-scale structure in turbulent mixing layers," J. Fluid Mech. **199**, 297 (1989).

[6]F. Gao, and E.E. O'Brien, "Direct numerical simulation of reacting flows in homogeneous turbulence," AIChE J. **37**, 1459 (1991).

[7]P. Givi, C.K. Madnia, C.J. Steinberger, M.H. Carpenter,and J.P. Drummond, "Effects of compressibility and heat release in a high speed reacting mixing layer," Combust. Sci. Tech. **78**, 33 (1991).

[8]F.F. Grinstein, and K. Kailasanath, "Chemical energy release and dynamics of transitional, reactive shear flows," Phys. Fluids A **4**, 2207 (1992).

[9]C.J. Montgomery, G. Kosály, and J.J. Riley, "Direct numerical simulation of turbulent reacting flow using a reduced hydrogen-oxygen mechanism," Combust. Flame **95**, 247 (1993).

[10]R.S. Miller, K. Madnia, and P. Givi, "Structure of a turbulent reacting mixing layer," Combust. Sci. Tech. **99**, 1 (1994).

[11]Y.Y. Lee, and S.B. Pope, "Nonpremixed turbulent reacting flow near extinction," Combust. Flame **101**, 501 (1995).

[12]N. Swaminathan, S. Mahalingam, and R.M. Kerr, "Structure of nonpremixed reaction zones in numerical isotropic turbulence," Theoret. Comput. Fluid Dynamics **8**, 201 (1996).

[13]C.J. Montgomery, G. Kosály, and J.J. Riley, "Direct numerical simulation of turbulent reacting flow using a reduced hydrogen-oxygen mechanism," Combust. Flame **109**, 113 (1997).

[14]F.A. Javery, R.S. Miller, F. Mashayek, and P. Givi, "Differential diffusion in binary scalar mixing and reaction," Combust. Flame **109**, 561 (1997).

[15]S. Lee, S.K. Lele, and P. Moin, "Eddy-shocklets in decaying compressible turbulence," Phys. Fluids **3**, 657 (1991).

[16]W.C. Reynolds, "The potential and limitations of direct and large eddy simulations," Lect. Notes Phys. **357**, 313 (1991).

[17]J.R. Ristorcelli, and G.A. Blaisdell, "Consistent initial conditions for the DNS of compressible turbulence," Phys. Fluids **9**, 4 (1997).

[18]G.A. Blaisdell, and J.R. Ristorcelli, "Consistent initial conditions for the DNS of compressible turbulence," APS Division of Fluid Dynamics Meeting (1996).

[19]S. Tavoularis, J.C. Bennett, and S. Corrsin, "Velocity derivative skewness in small Reynolds number nearly isotropic turbulence," J. Fluid Mech. **88**, 63 (1978).

[20]S.A. Orszag, and J.S. Patterson, "Numerical simulation of three-dimensional homogeneous isotropic turbulence," Phys. Rev. Lett. **28**, 76 (1972).

[21]R.N. Gupta, J.M. Yos, R.A. Thompson, and K. Lee, "A review of reaction rates and thermodynamic and transport properties for an 11-species air model for chemical and thermal non-equilibrium calculations to 30,000 K," NASA RP-1260 (1990).

[22]J.E. Moyal, "The spectra of turbulence in a compressible fluid; eddy turbulence and random noise," Proc. Cambridge Phil. Soc. **48**, 329 (1951).

[23]P. Moin, "Progress in large eddy simulation of turbulent flows," AIAA Paper No. 97-0749 (1997).

[24]R.A. Greenberg, "Non-equilibrium vortex flow in a dissociating gas," J. Aerospace Sci. **29**, 1484 (1962).

[25]A.Q. Eschenroeder, "Intensification of turbulence by chemical heat release," Phys. Fluids **7**, 1735 (1964).

Figure Captions

FIGURE 1. Time evolution of the average N_2 mass fraction for simulations of recombining nitrogen atoms at initial $M_t = 0.519$, $Re_\lambda = 34.5$, and $\overline{\Delta h^\circ} = 33$, 16, 13, and 9, corresponding to initial $T_\circ = 2000$, 4000, 5000, and 7000 K respectively.

FIGURE 2. Time evolution of (a) average temperature; (b) turbulent kinetic energy; and (c) relative compressible kinetic energy showing the effect of $\overline{\Delta h^\circ}$ for $Da = 1$, $M_t = 0.346$, and $Re_\lambda = 34.5$.

FIGURE 3. Three-dimensional incompressible, E^I, and compressible, E^C, shell-averaged energy spectra for (a) non-reacting; (b) endothermic ($\overline{\Delta h^\circ} = -1$); and (c) exothermic ($\overline{\Delta h^\circ} = 2$) simulations for $Da = 1$, $M_t = 0.346$, and $Re_\lambda = 34.5$.

FIGURE 4. Three-dimensional incompressible, E^I, and compressible, E^C, shell-averaged energy spectra for non-reacting and exothermic ($\overline{\Delta h^\circ} = 2$) simulations for $Da = 1$, $M_t = 0.346$, and $Re_\lambda = 34.5$ at $t/\tau_t = 1.5$.

FIGURE 5. Time evolution of RMS temperature fluctuations showing the effect of $\overline{\Delta h^\circ}$ for $Da = 1$, $M_t = 0.346$, and $Re_\lambda = 34.5$.

FIGURE 6. Time evolution of (a) average mass fraction of reactants; (b) turbulent kinetic energy; and (c) RMS temperature fluctuations showing the effect of Da for $\overline{\Delta h^\circ} = 1$, $M_t = 0.346$, and $Re_\lambda = 34.5$.

FIGURE 7. Time evolution of the RMS temperature fluctuations showing the effect of M_t for $\overline{\Delta h^\circ} = 1$, $Da = 1$, and $Re_\lambda = 34.5$.

FIGURE 8. Normalized vorticity, $\vec{\omega}_t \tau_t / \omega_\circ$, budget for non-reacting (empty symbols) and (a) exothermic ($\overline{\Delta h^\circ} = 2$) (filled symbols); and (b) endothermic ($\overline{\Delta h^\circ} = -1$) (filled symbols) simulations for $Da = 1$, $M_t = 0.346$, and $Re_\lambda = 34.5$; ($\square$), stretching production; ($\triangle$), compressible destruction; ($\bigcirc$), non-reacting entropy production; ($\diamond$), reacting entropy production.

FIGURE 9. Time evolution of vorticity magnitude showing the effect of $\overline{\Delta h^\circ}$ for $M_t = 0.346$, $Re_\lambda = 34.5$, and $Da = 1$.

FIGURE 10. Normalized Reynolds stress, $R_{22,t}/\epsilon_o$, budget for non-reacting (empty symbols) and exothermic (filled symbols) simulations for $M_t = 0.346$, $Re_\lambda = 34.5$, $Da = 1$, and $\overline{\Delta h^\circ} = 2$; ($\diamond$), pressure-strain; ($\bigtriangledown$), viscous diffusion; ($\bigtriangleup$), dissipation.

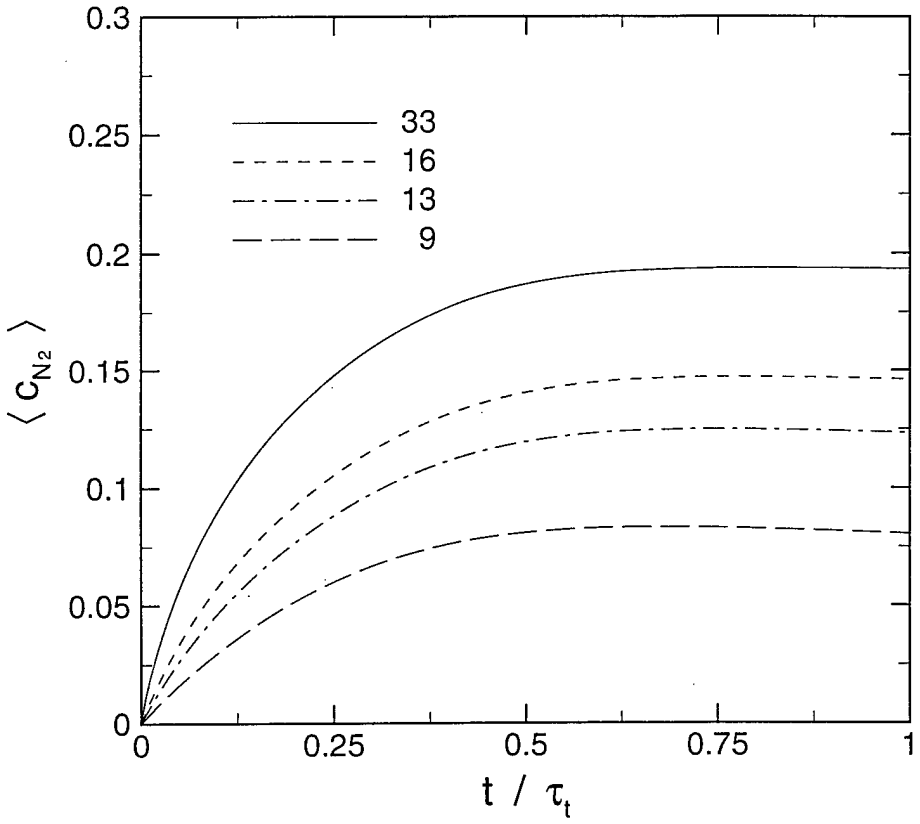

FIG. 1)

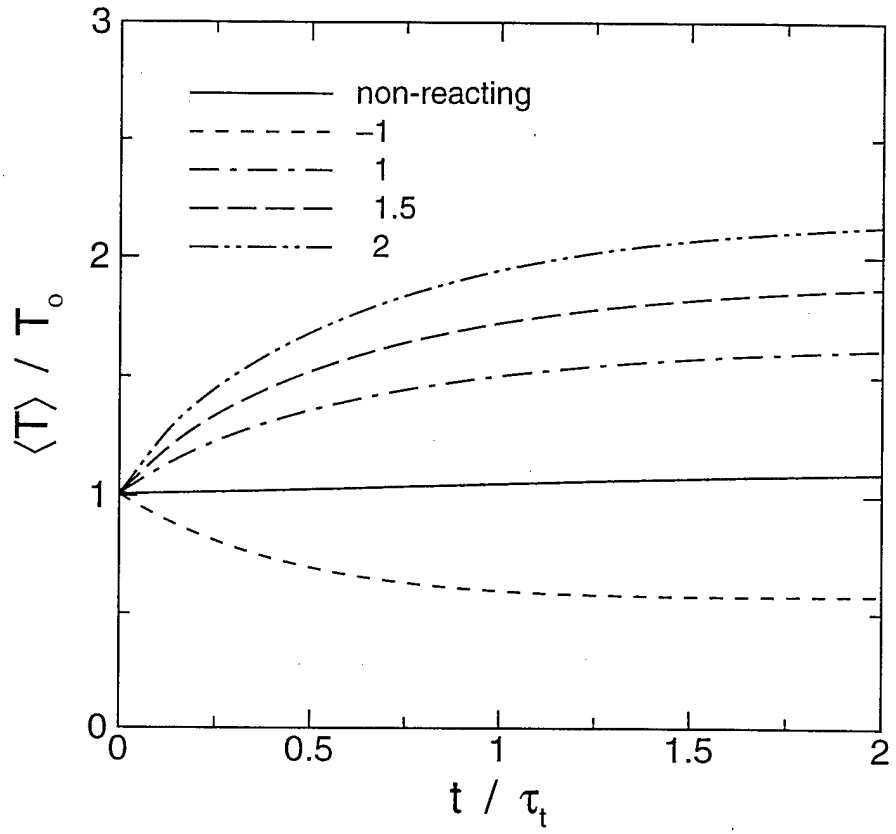

FIG. 2 a)

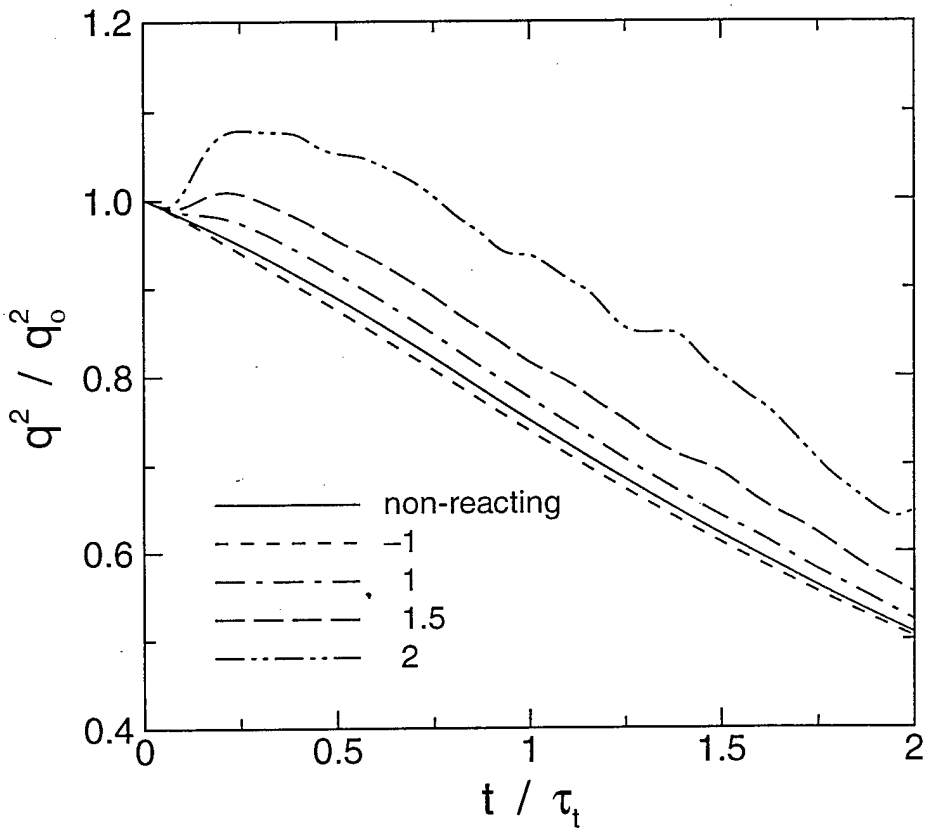

FIG. 2 b)

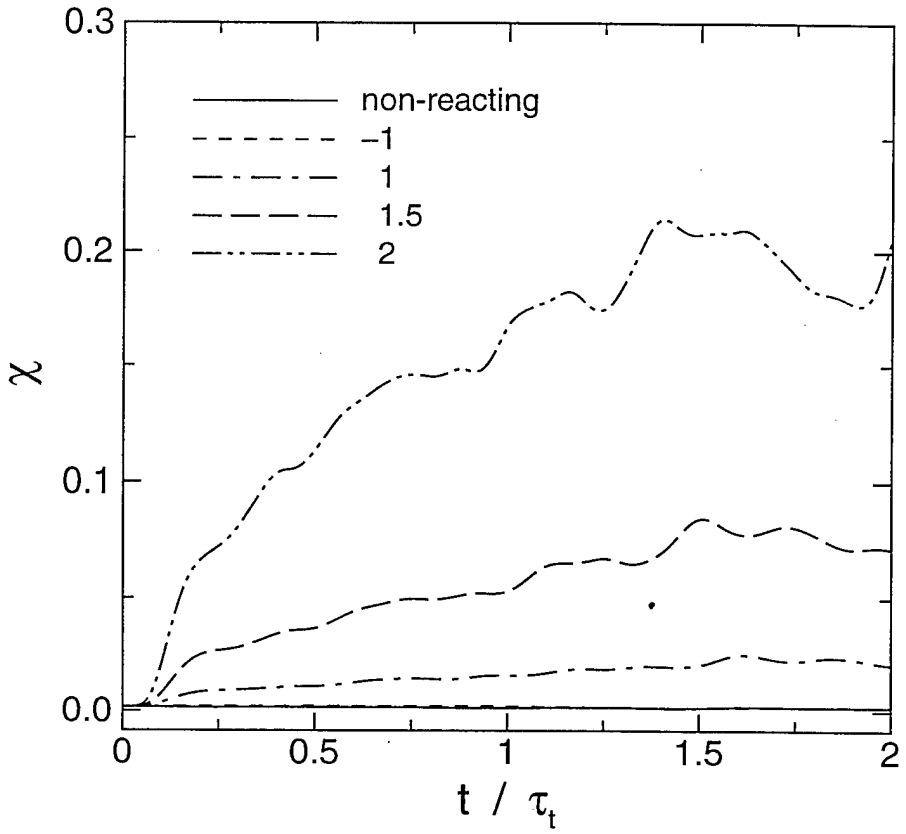

FIG. 2 c)

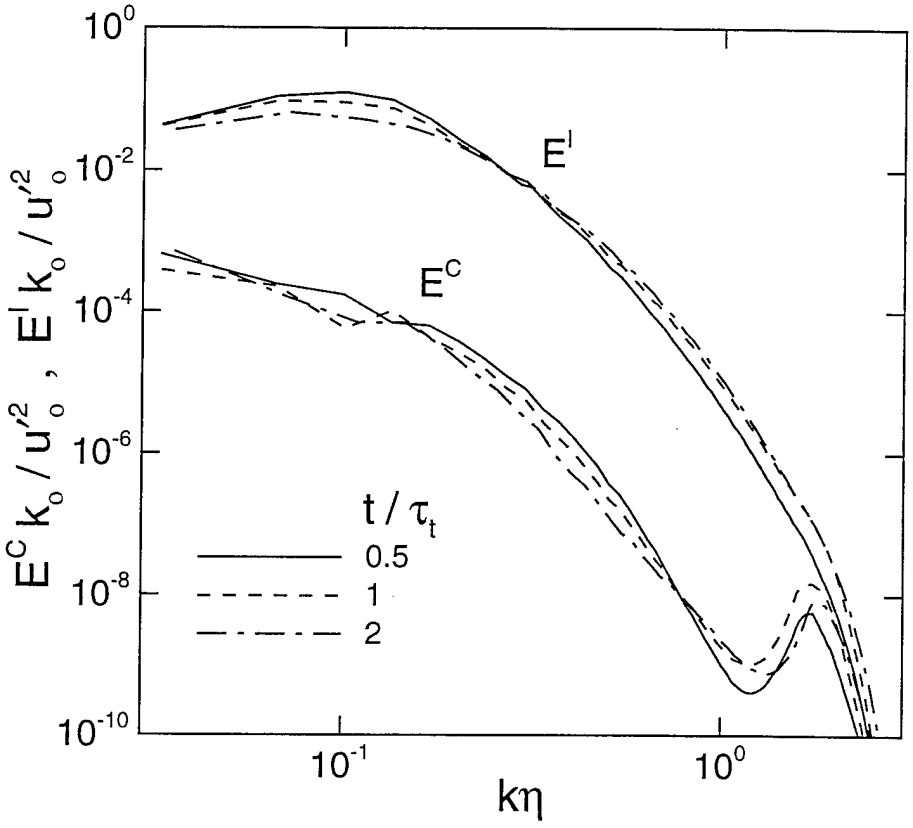
10^0
10^{-2}
10^{-4}
10^{-6}
10^{-8}
10^{-10}
$E^C k_o / u'^2_o$, $E^I k_o / u'^2_o$
E^I
E^C
t / τ_t
0.5
1
2
10^{-1}
10^0
$k\eta$

FIG. 3 a)

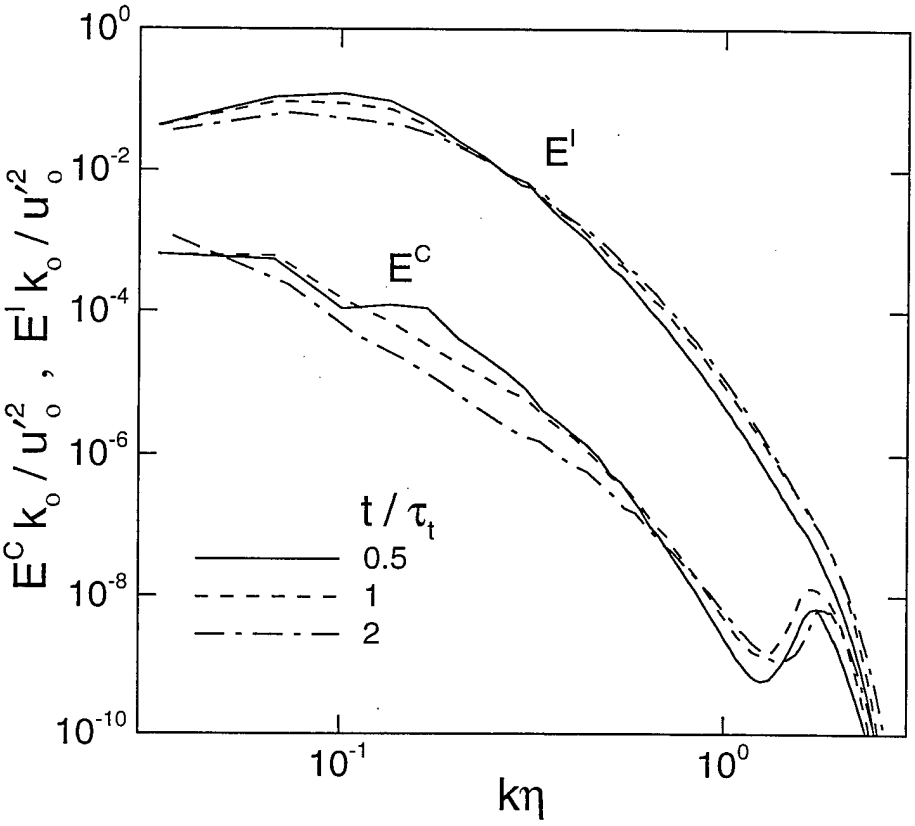
10^0
10^{-2}
10^{-4}
10^{-6}
10^{-8}
10^{-10}
$E^C k_o / u'^2_o$, $E^I k_o / u'^2_o$
E^I
E^C
t / τ_t
0.5
1
2
10^{-1}
10^0
$k\eta$

FIG. 3 b)

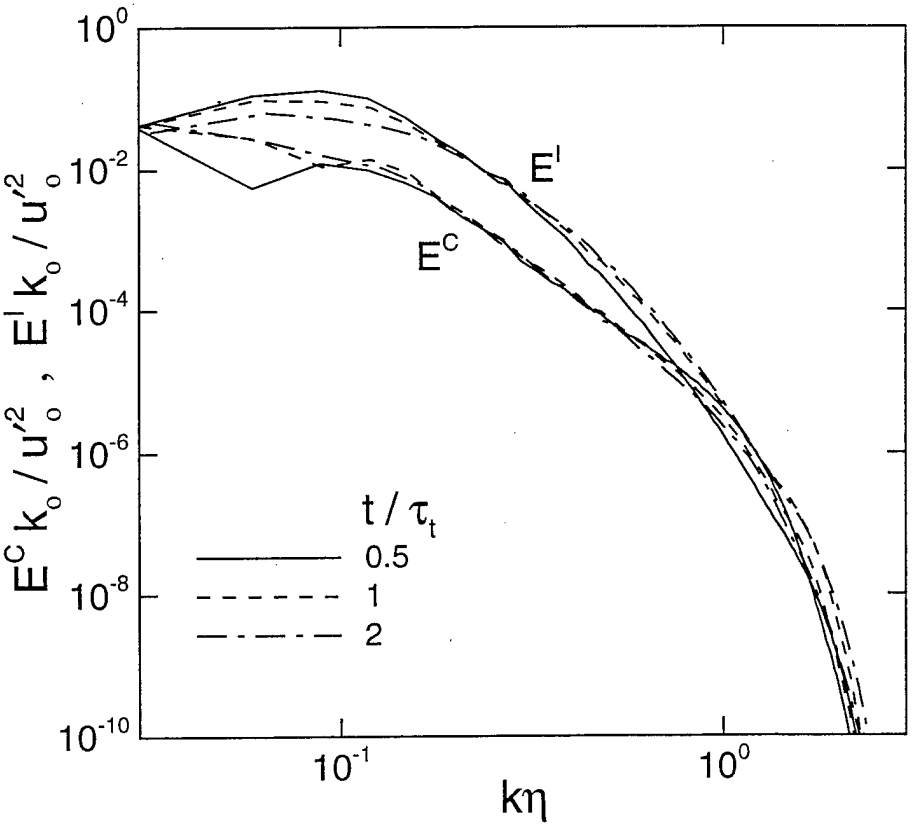
10^0
10^{-2}
10^{-4}
10^{-6}
10^{-8}
10^{-10}
$E^C k_o / u'^2_o$, $E^l k_o / u'^2_o$
E^l
E^C
t / τ_t
0.5
1
2
10^{-1}
10^0
$k\eta$

FIG. 3 c)

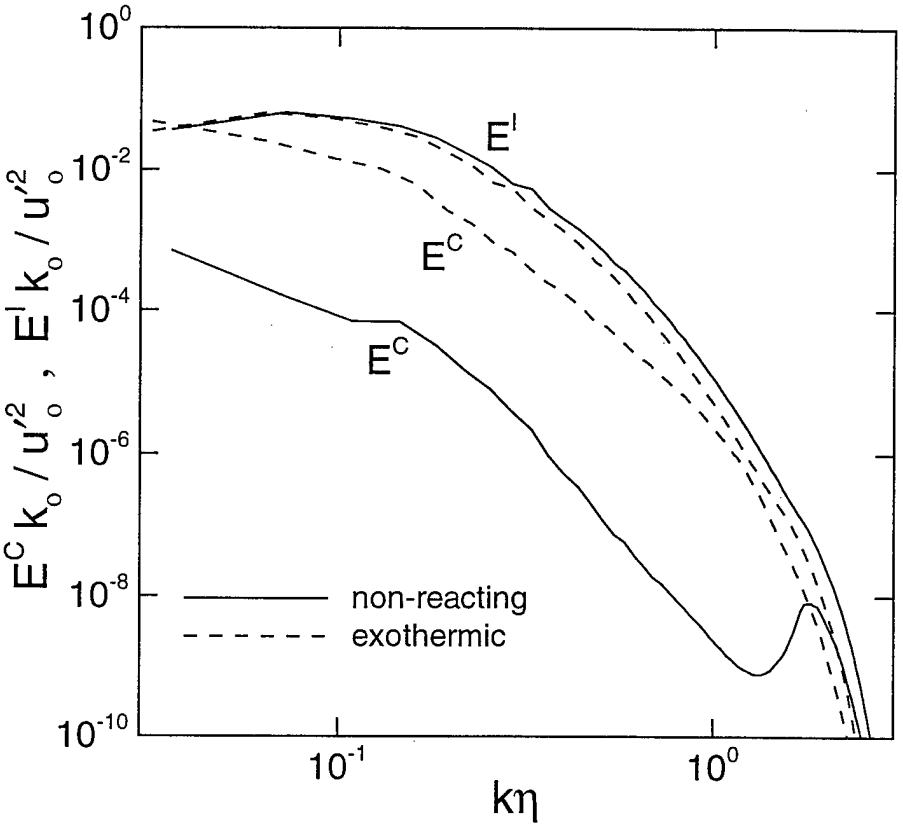
10^0
10^{-2}
10^{-4}
10^{-6}
10^{-8}
10^{-10}
$E^C k_o / u'^2_o$, $E^I k_o / u'^2_o$
E^I
E^C
E^C
non-reacting
exothermic
10^{-1}
10^0
$k\eta$

FIG. 4

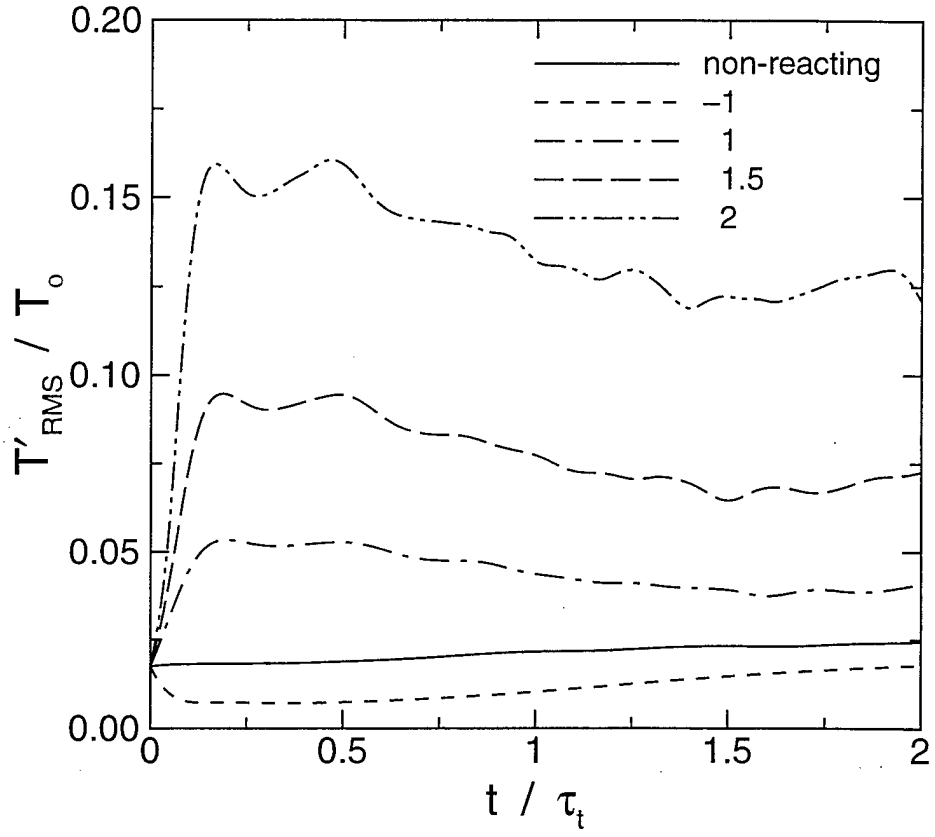

FIG. 5

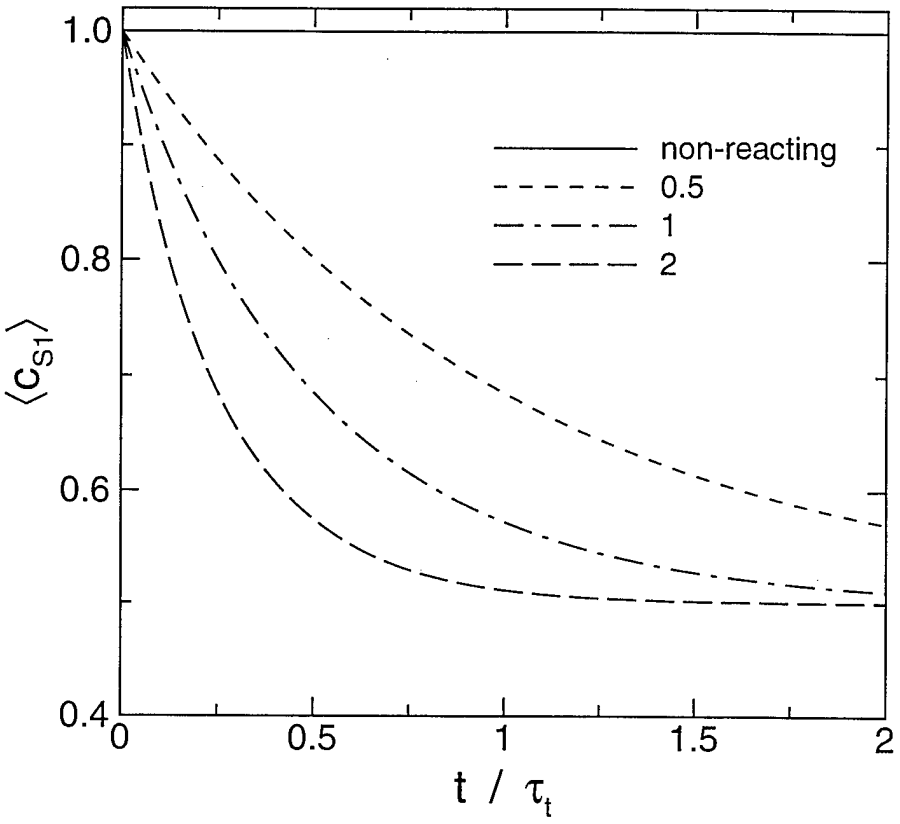
1.0
0.8
0.6
0.4
0
0.5
1
1.5
2
$\langle c_{S1} \rangle$
t / τ_t
non-reacting
0.5
1
2

FIG. 6 a)

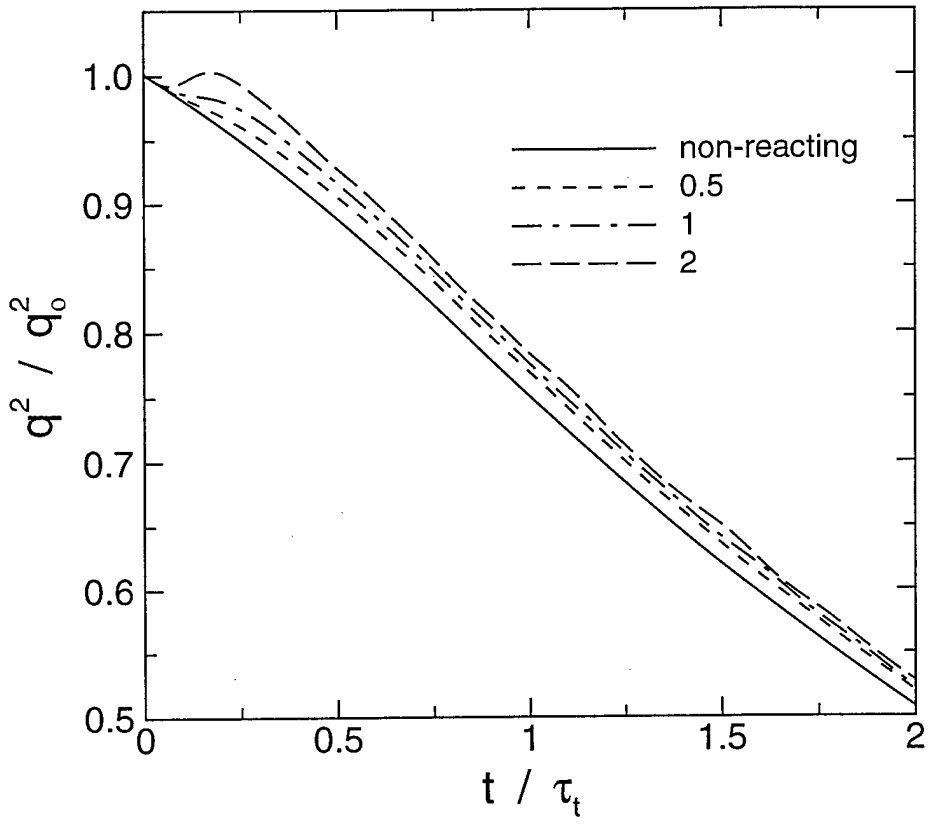

FIG. 6 b)

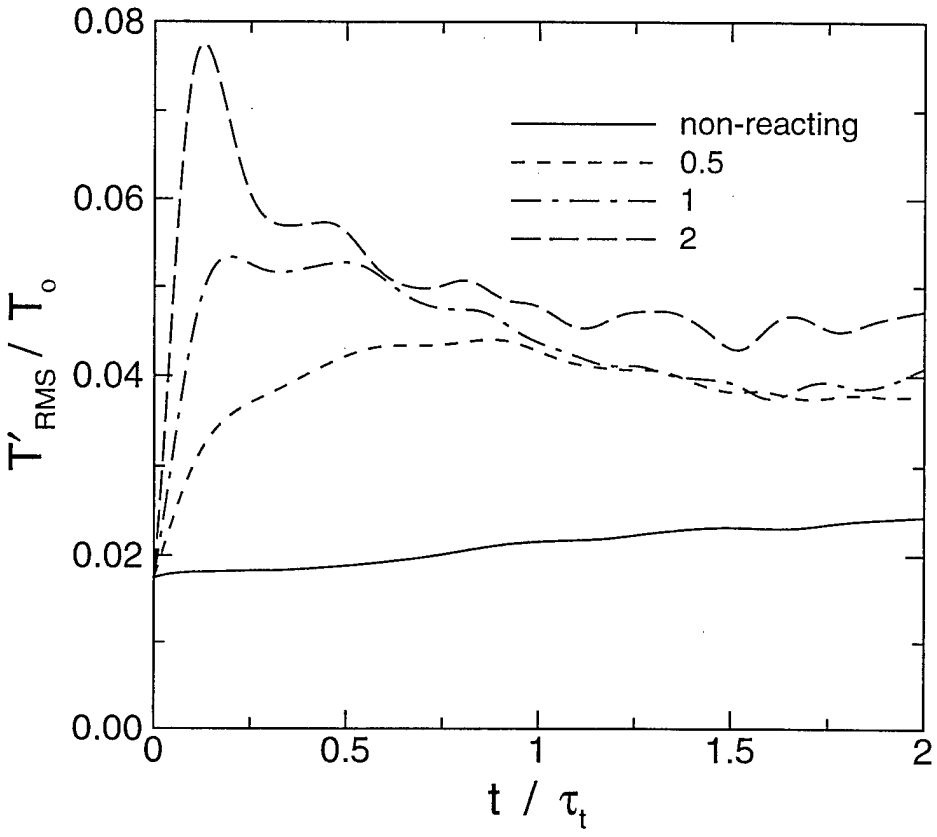

FIG. 6 c)

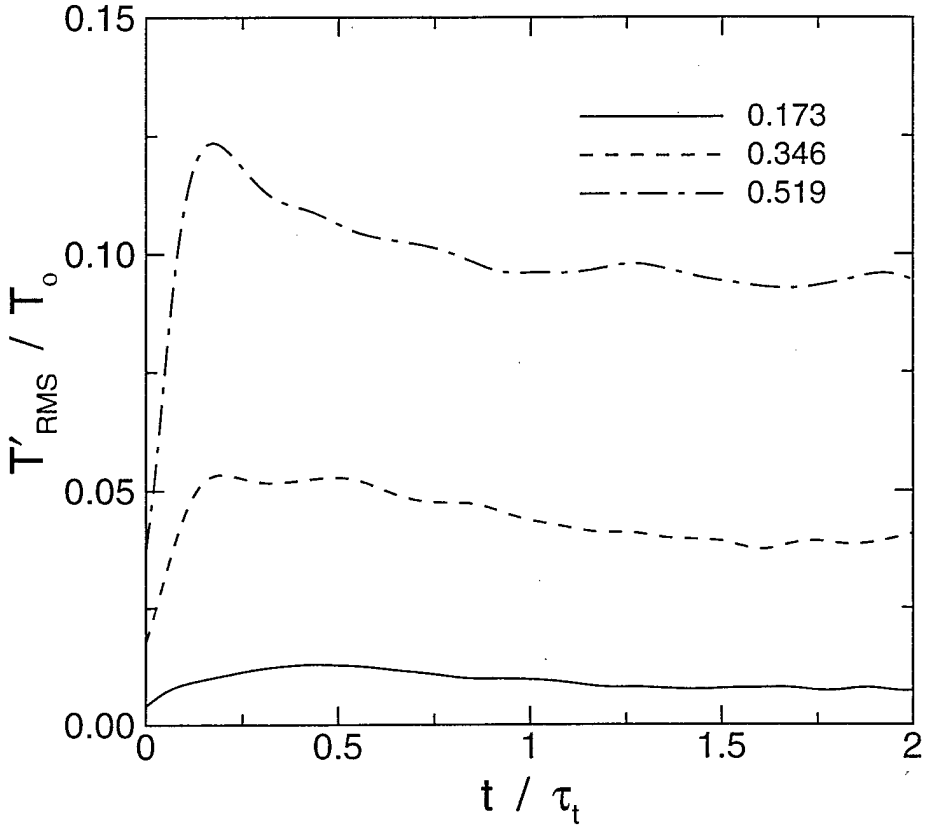

FIG. 7

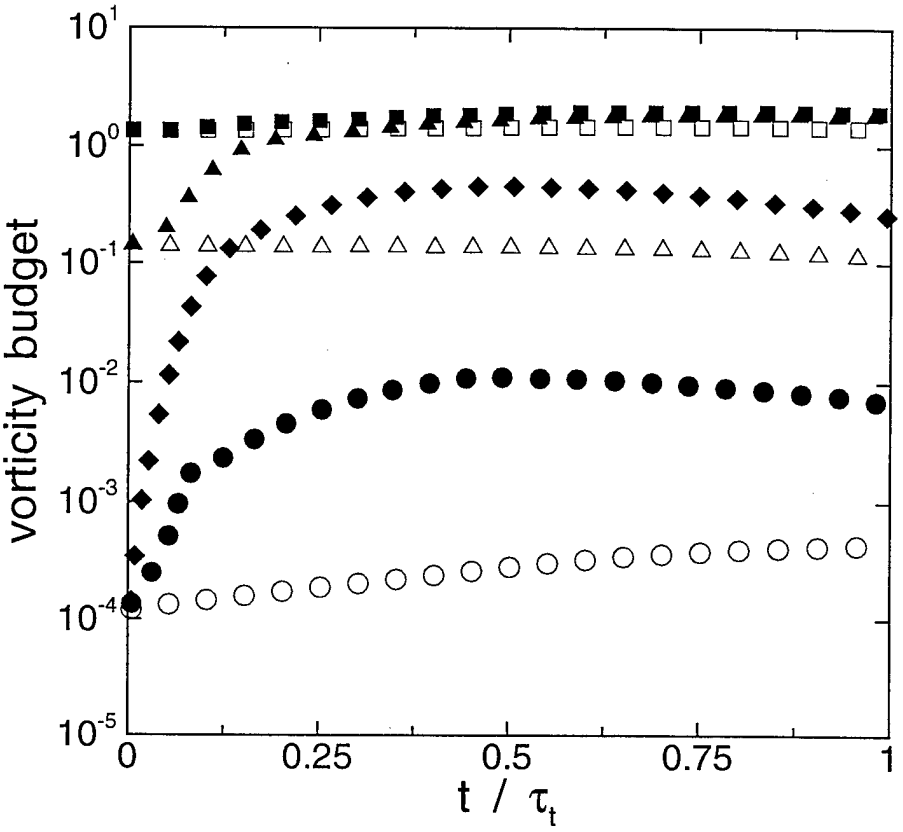
vorticity budget
10^{1}
10^{0}
10^{-1}
10^{-2}
10^{-3}
10^{-4}
10^{-5}
0
0.25
0.5
0.75
1
t / τ_t

FIG. 8 a)

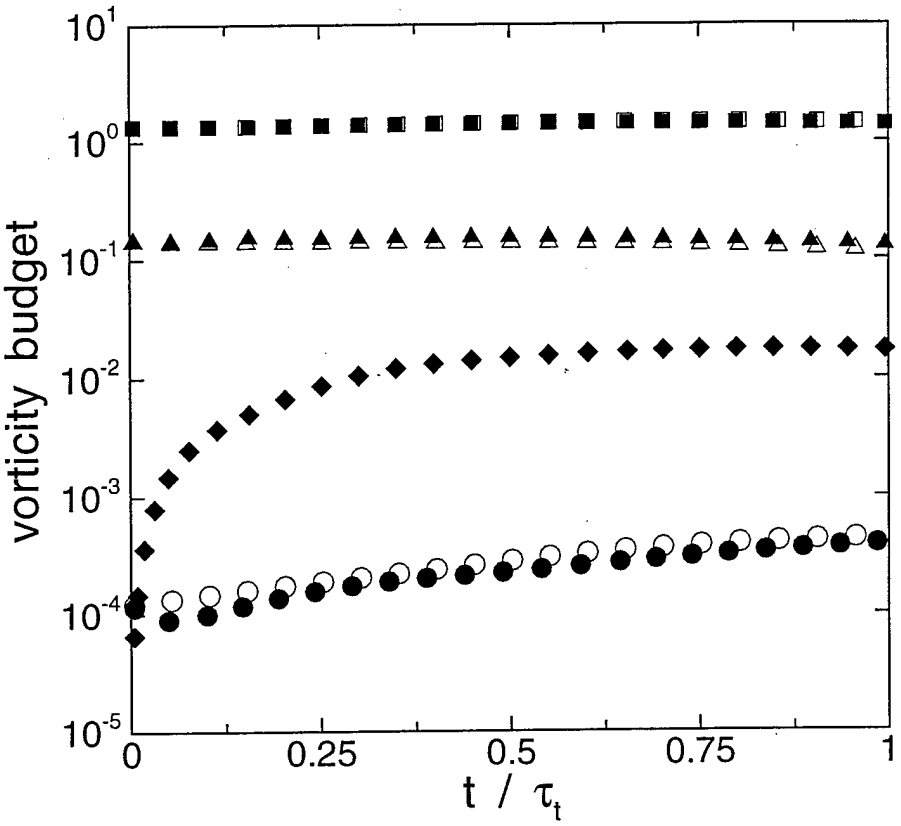
vorticity budget
10^{1}
10^{0}
10^{-1}
10^{-2}
10^{-3}
10^{-4}
10^{-5}
0
0.25
0.5
0.75
1
t / τ_t

FIG. 8 b)

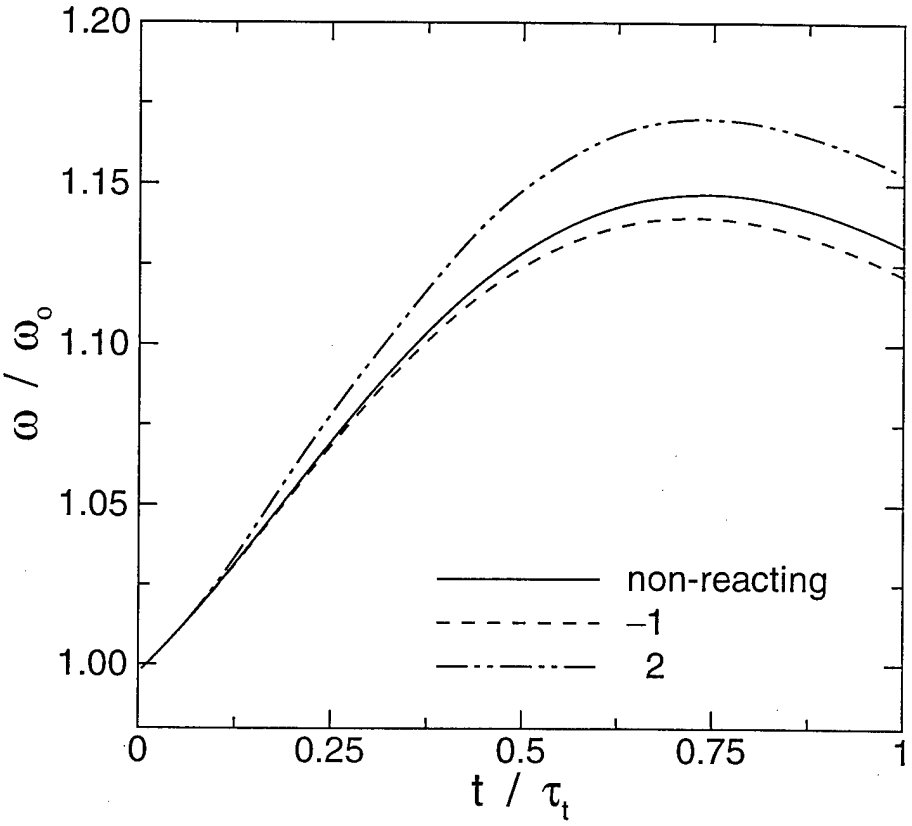

FIG. 9

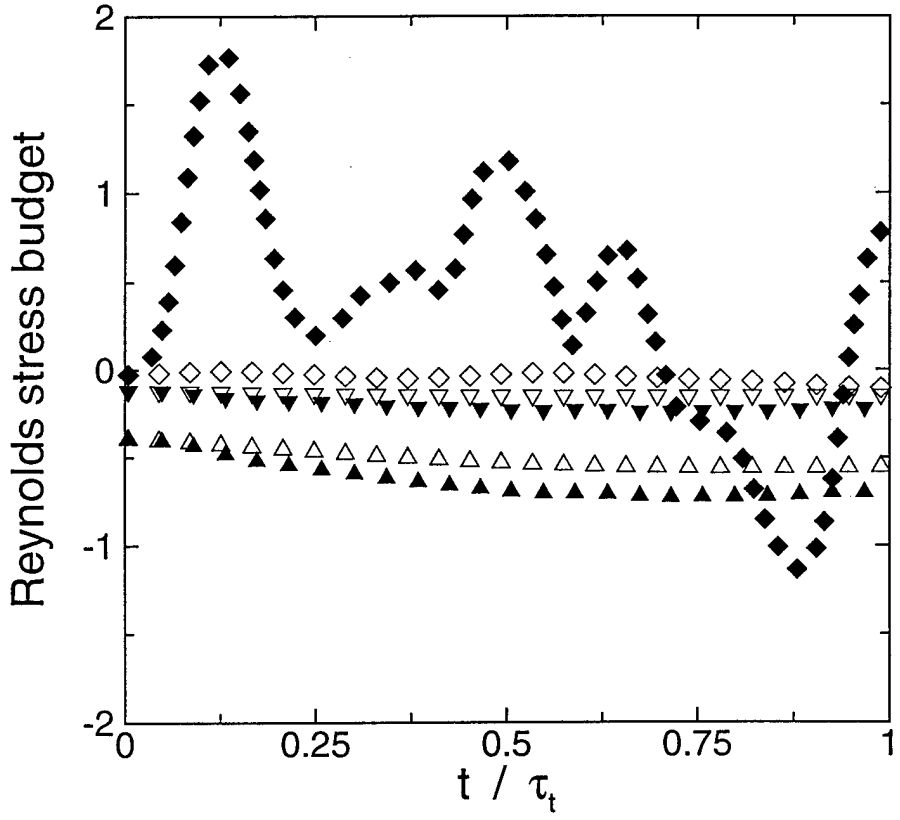

FIG. 10

Subgrid-Scale Model for the Temperature Fluctuations in Reacting Turbulence

M. Pino Martín

Graham V. Candler

Department of Aerospace Engineering and Mechanics
University of Minnesota
110 Union St. SE, Minneapolis, MN 55455

candler@aem.umn.edu

A direct numerical simulation database is used to develop a model of subgrid-scale temperature fluctuations for use in large-eddy simulations of turbulent, reacting hypersonic flows. In these flows, the reaction rate varies exponentially with temperature, and thus small temperature fluctuations may cause large fluctuations in the rate of product formation. The proposed model uses a probability density representation of the temperature fluctuations. The DNS database reveals a physically consistent relation between the resolved-scale flow conditions that may be used to predict the standard deviation of the Gaussian PDF. The model is calibrated and tested by comparison to simulations of decaying isotropic turbulence. The conditional single-variable PDF model is found to capture the fluctuations in temperature and product formation.

Introduction

The boundary layer on proposed air-breathing hypersonic cruise vehicles will be turbulent and chemically reacting. To aid the design of such vehicles, an accurate CFD tool is required. Currently, the computer cost dissuades the usage of direct numerical simulations (DNS) of hypersonic flows at realistic Reynolds numbers, at the same time that it encourages the use of large-eddy simulations (LES). Therefore, subgrid-scales (SGS) models need to be devised to close the turbulence-chemistry interaction in LES of hypersonic flows.

Much work has been done in modeling turbulent reacting flows.[1–10] However, most of this work has been focused on combustion related applications, where fluctuations in the chemical source term are mainly caused by fluctuations in the species mass fraction. In hypersonic flows, the equilibrium composition of reacting air depends strongly on the temperature. Furthermore, the reactions are temperature limited and the reaction rate depends exponentially on temperature. With the very high energies present in hypersonic flows, the temperature fluctuations will be very large, and result in large increases in

the reaction rates. Therefore, in hypersonic flows the temperature fluctuations must be modeled to obtain accurate reaction rates and product formation.

In LES, it is generally assumed that the small scales are more isotropic and more universal in character for different flows than the large scales. Therefore, it is customary to develop SGS models in isotropic turbulence, for later use in the more complex flows. In our previous work,[11] we studied the interaction between decaying isotropic turbulence and finite-rate chemical reactions at conditions typical of a hypersonic boundary layer. The results confirmed that the interaction is characterized by the increased or decreased magnitude of the temperature fluctuations for exothermic or endothermic reactions, respectively.

In this paper, we use the DNS database of isotropic reacting turbulence to develop and evaluate a model for the temperature fluctuations. Our approach builds on the reaction rate modeling for combustion applications. In particular, Gaffney *et al.*[8] assume a probability density function (PDF) for the temperature fluctuations and investigate how the fluctuations affect the combustion process. The proposed model has a similar form, however we use the results of DNS to calibrate the model. Therefore, the parameters that describe the PDF are based on detailed turbulence data. This model represents the unresolved (subgrid-scale) fluctuations for use in large-eddy simulations of turbulence, where the small scales are assumed to be isotropic. As reactions, we use either dissociating nitrogen molecules or dissociating oxygen molecules. These are primary reactions that occur in hypersonic boundary layers.

In the remainder of the paper, we review the governing equations, we Favre average these equations and show that the unresolved temperature fluctuations must be modeled for large-eddy simulations. We then discuss the data analysis for the prediction of the temperature fluctuations, and evaluate the results by comparison with the DNS results.

Governing equations

The equations describing the unsteady motion of a reacting flow with no contribution of vibrational modes are given by the species mass, mass-averaged momentum, and total energy conservation equations

$$\begin{aligned}
\frac{\partial \rho_s}{\partial t} + \frac{\partial}{\partial x_j}\Big(\rho_s u_j + \rho_s v_{sj}\Big) &= w_s \\
\frac{\partial \rho u_i}{\partial t} + \frac{\partial}{\partial x_j}\Big(\rho u_i u_j + p\delta_{ij} - \tau_{ij}\Big) &= 0 \qquad (1) \\
\frac{\partial E}{\partial t} + \frac{\partial}{\partial x_j}\Big((E+p)u_j - u_i\tau_{ij} + q_j + \sum_s \rho_s v_{sj} h_s\Big) &= 0
\end{aligned}$$

where ρ_s is the density of species s; w_s represents the rate of production of species s due to chemical reactions; ρ_s is the density of species s; u_j is the mass-averaged velocity in the j direction; v_{sj} is the diffusion velocity of species s; ρ is the sum over species s density; p is the pressure; τ_{ij} is the shear stress tensor given by a linear stress-strain relationship; q_j is the heat flux due to temperature gradients; h_s is the specific enthalpy of species s; and E is the total energy per unit volume given by

$$E = \sum_s \rho_s c_{vs} T + \tfrac{1}{2}\rho u_i u_i + \sum_s \rho_s h_s^\circ, \tag{2}$$

where c_{vs} is the specific heat at constant volume of species s; and h_s° represents the heat of formation of species s.

We consider a simple reaction system: dissociating nitrogen molecules. This is one of the primary reactions that occur in hypersonic boundary layers, but more importantly, it serves as a good example for the form of the chemical source term. The dissociation reaction may be written symbolically as:

$$\mathrm{N_2 + M \rightleftharpoons 2N + M}, \tag{3}$$

where M represents a collision partner, which is either N_2 or N in this case. The source terms for N_2 and N can be written using the law of mass action

$$\begin{aligned} w_{\mathrm{N_2}} &= -M_{\mathrm{N_2}} k_f \Big(\frac{\rho_{\mathrm{N_2}}}{M_{\mathrm{N_2}}}\Big)\Big(\frac{\rho_{\mathrm{N_2}}}{M_{\mathrm{N_2}}} + \frac{\rho_{\mathrm{N}}}{M_{\mathrm{N}}}\Big) + M_{\mathrm{N_2}} k_b \Big(\frac{\rho_{\mathrm{N}}}{M_{\mathrm{N}}}\Big)^2 \Big(\frac{\rho_{\mathrm{N_2}}}{M_{\mathrm{N_2}}} + \frac{\rho_{\mathrm{N}}}{M_{\mathrm{N}}}\Big) \\ &= w_{f\mathrm{N_2}} + w_{b\mathrm{N_2}}, \end{aligned} \tag{4}$$

and $w_{\mathrm{N_2}} = -w_{\mathrm{N}}$. k_f and k_b are the forward and backward reaction rates respectively; These are written as

$$\begin{aligned} k_f &= C\, T^\eta\, e^{-\theta/T}, \\ k_b &= \frac{k_f}{K_{eq}}, \end{aligned} \tag{5}$$

where C, η, and θ are experimentally-determined constants,[12] and K_{eq} is the known temperature-dependent equilibrium constant.[13]

For a two-species mixture, the diffusion velocity can be accurately represented using Fick's law

$$\rho_s v_{sj} = -\rho D \frac{\partial c_s}{\partial x_j}, \tag{6}$$

where $c_s = \rho_s/\rho$ is the mass fraction, and D is the diffusion coefficient given in terms of the Lewis number

$$Le = \frac{\rho D Pr}{\mu}, \tag{7}$$

where Pr is the Prandtl number, μ is the viscosity, and Le is taken to be unity, so that the energy transport due to mass diffusion is equal to the energy transport due to thermal conduction.

Favre average of conservation equations

To discuss how the conservation equations must be modeled, we need to separate the resolvable fluctuations from those that the grid cannot resolve. In compressible flows, it is convinient to use Favre-filtering to avoid the introduction of subgrid-scale terms in the equation of conservation of mass. A Favre-filtered variable is defined as:

$$\tilde{f} = \frac{\overline{\rho f}}{\bar{\rho}}. \tag{8}$$

where the over-bar denotes a filtering operation that maintains only the large-scales. Accordingly, the Favre-filtered equations describing the unsteady motion of a reacting flow with no contribution of vibrational modes are given by the species mass, momentum, and total energy equations:

$$\begin{aligned}
&\frac{\partial}{\partial t}(\bar{\rho}\tilde{c}_s) + \frac{\partial}{\partial x_j}\Big(\bar{\rho}\tilde{c}_s\tilde{u}_j + \bar{\rho}\tilde{v}_{sj} + V_{sj}\Big) = \tilde{w}_s \\
&\frac{\partial}{\partial t}(\bar{\rho}\tilde{u}_i) + \frac{\partial}{\partial x_j}\Big(\bar{\rho}\tilde{u}_i\tilde{u}_j + \tilde{p}\delta_{ij} + \tau_{ij} - \tilde{\sigma}_{ij}\Big) = 0 \\
&\frac{\partial \tilde{E}}{\partial t} + \frac{\partial}{\partial x_j}\Big((\tilde{E}+\bar{p})\tilde{u}_j - \tilde{\sigma}_{ij}\tilde{u}_j + \tilde{q}_j + \bar{\rho}\sum_s \tilde{c}_s\tilde{v}_{sj}\tilde{h}_s + \tilde{\gamma}Q_j + \Sigma_j + \sum_s h_s^{\circ}V_{sj}\Big) = 0
\end{aligned} \tag{9}$$

where $\tilde{c}_s = \tilde{\rho}_s/\bar{\rho}$ is the Favre-averaged mass fraction, and the SGS diffusion velocity has been introduced

$$V_{sj} = \bar{\rho}\Big(\widetilde{c_s u_j} - \tilde{c}_s\tilde{u}_j\Big) \ . \tag{10}$$

In the momentum equation, τ_{ij} is the SGS stress

$$\tau_{ij} = \bar{\rho}\Big(\widetilde{u_i u_j} - \tilde{u}_i\tilde{u}_j\Big) \ , \tag{11}$$

and $\tilde{\sigma}_j$ has been simplified according to

$$\tilde{\sigma}_j = \tilde{\mu}\frac{\partial \tilde{u}_i}{\partial x_j} + \tilde{\mu}\frac{\partial \tilde{u}_j}{\partial x_i} - \frac{2}{3}\tilde{\mu}\frac{\partial \tilde{u}_k}{\partial x_k}\delta_{ij} \ , \tag{12}$$

thus, the viscosity is assumed to be a weak function of the mixture mole fractions, and its fluctuations are neglected. In the energy equation, we have introduced the average ratio of specific heats, $\tilde{\gamma}$, the SGS heat flux

$$Q_j = \bar{\rho}\Big(\widetilde{u_j T} - \tilde{u}_j\tilde{T}\Big) \ , \tag{13}$$

and the SGS kinetic energy flux

$$\Sigma_j = \frac{\bar{\rho}}{2}\Big(u_k\widetilde{u_k u_j} - \tilde{u}_k\tilde{u}_k\tilde{u}_j\Big) \ . \tag{14}$$

These terms are derived by considering the Favre average of the energy-velocity product

$$\begin{aligned}\widetilde{Eu_j} &= \bar{\rho}\Sigma_s c_{vs}\widetilde{c_s u_j}T + \frac{1}{2}\bar{\rho}u_k\widetilde{u_k u_j} + \bar{\rho}\Sigma_s h^\circ\widetilde{c_s u_j} \\ &= \tilde{E}\tilde{u}_j + \Sigma_j + \Sigma_s h_s^\circ V_{sj} + \bar{\rho}\Sigma_s c_{vs}\Big(\widetilde{c_s T u_j} - \tilde{c}_s\tilde{T}\tilde{u}_j\Big) \\ &\approx \tilde{E}\tilde{u}_j + \tilde{\gamma}Q_j + \Sigma_j + \Sigma_s h_s^\circ V_{sj}\end{aligned} \tag{15}$$

where we have assumed that the mass fraction fluctuations are not directly correlated with the temperature-velocity variations. The energy gives the temperature

$$\tilde{E} = \bar{\rho}\tilde{\gamma}\tilde{T} + \frac{1}{2}\bar{\rho}\tilde{u}_i\tilde{u}_i + \bar{\rho}\Sigma_s h_s^\circ\tilde{c}_s + \bar{\rho}\Sigma_s c_{vs}\Phi_s + \frac{1}{2}\tau_{ij} \ , \tag{16}$$

where $\Phi_s = \widetilde{Tc_s} - \tilde{T}\tilde{c}_s$. And the pressure is given by

$$\bar{p} = \bar{\rho}R\tilde{T} + \bar{\rho}R\Sigma_s\Phi_s \ . \tag{17}$$

The results from DNS of isotropic turbulence show that the terms involving the SGS temperature-species correlation, Φ_s, are negligible in comparison to the rest of the terms in the equations of state and total energy. Thus, if this result prevails in the case of the hypersonic boundary layer, Φ_s will drop out in the large eddy simulations.

Finally we must consider the chemical source term, $\tilde{w}_s$, in the continuity equation. The strong temperature-dependence of the source term can be seen by representing the variables as their Favre-averaged and subgrid-scale values: $T = \tilde{T} + T^{sgs}$ and $c_s = \tilde{c}_s + c_s^{sgs}$. The source term (4) to first order in the subgrid-scale quantities is:

$$\begin{aligned}w_{f\mathrm{N}_2} &= \tilde{w}_{f\mathrm{N}_2} + \tilde{w}_{f\mathrm{N}_2}\Big(\big(\frac{\theta}{\tilde{T}} + \eta\big)\frac{T^{sgs}}{\tilde{T}} + c_{\mathrm{N}_2}^{sgs}\Big) + \dots \\ w_{b\mathrm{N}_2} &= \tilde{w}_{b\mathrm{N}_2} + \tilde{w}_{b\mathrm{N}_2}\Big(\big(\frac{\theta}{\tilde{T}} + \eta\big)\frac{T^{sgs}}{\tilde{T}} - 2c_{\mathrm{N}_2}^{sgs}\Big) + \dots\end{aligned} \tag{18}$$

where we have made use of the fact that $c_{\mathrm{N}}^{sgs} = -c_{\mathrm{N}_2}^{sgs}$, and we have assumed that the variation of K_{eq} in temperature is relatively weak, which is a good approximation at very high temperatures. The variations of w_{N_2} caused by temperature fluctuations may be especially large because θ is typically an order of magnitude larger than the temperature. Thus, to obtain accurate $\tilde{w}_s$ we must model the subgrid-scale temperature fluctuations.

This derivation shows that the following terms must be modeled:

$$\begin{aligned} V_{sj} &= \text{SGS diffusion of species s,} \\ \tau_{ij} &= \text{SGS stress,} \\ Q_j &= \text{SGS heat flux,} \\ \Sigma_j &= \text{SGS kinetic energy flux,} \\ T^{sgs} &= \text{SGS temperature fluctuations.} \end{aligned} \tag{19}$$

Much work has been done in modeling τ_{ij} and Q_j,[14–18] whereas very little effort has been given to modeling V_{sj}, Σ_j, and T^{sgs}. However, Gao and O'Brien[19] briefly discuss the modeling of V_{sj} in the context of a dynamic SGS model, and Réveillon and Vervisch[20] discuss the modeling of Σ_j. The current paper includes the development of a model for T^{sgs}.

Simulations of reacting turbulence

In this section we present the numerical simulations for three-dimensional, compressible, homogeneous, isotropic, reacting turbulent flow. We use the same numerical method and isotropic initialization as Martín and Candler.[11] In particular, we use a sixth-order accurate finite difference scheme,[21] and a fourth-order accurate Runge-Kutta time integration. The simulations are performed on grids with 96^3. The fluctuating fields are initialized using Ristorcelli and Blaisdell[17] consistent initial conditions.

The non-dimensional parameters[11] governing the turbulence-chemistry interaction are the turbulent Reynolds number, the Mach number, the Damköhler number, the relative heat release and the equilibrium constant, namely

$$\begin{aligned} M_t &= \frac{q}{a}, & Re_\lambda &= \frac{\rho u' \lambda}{\mu}, \\ Da &= \frac{\tau_t}{\tau_c}, & \overline{\Delta h^\circ} &= -\frac{\Delta h^\circ}{c_v T + \frac{1}{2} q^2}, \end{aligned} \tag{20}$$

and K_{eq}^{13} is a non-dimensional function of the temperature and determines the equilibrium mixture composition. q is the RMS magnitude of the fluctuation velocity; a is the speed of sound; u' is the RMS turbulent velocity fluctuation in one direction; λ is the Taylor microscale; τ_t is the turbulent time scale; τ_c is the chemical time scale; and Δh° is the heat of the reaction.

We choose initial $Re_\lambda = 34.5$, $\langle \rho \rangle = 0.5$ kg/m^3, and $\langle T \rangle = 3000$ K for N_2 dissociation, and $\langle T \rangle = 2000$ K for O_2 dissociation. At these initial temperatures the reactions are

exothermic. We run simulations with combinations of initial $M_t = 0.35$, and 0.52, and N_2 or O_2 mass fractions in [0:1]. The various initial mass fraction conditions lead to distinct evolutions of the nonequilibrium chemistry. Therefore, different turbulent flow fields are obtained. The values of $\overline{\Delta h^\circ}$, Da, K_{eq}, and M_t vary physically during the simulations.

Prediction of temperature fluctuations

In this section, we describe the development of a model for the subgrid-scale temperature fluctuations. We represent the temperature fluctuations as a PDF.[23] During a LES we would obtain the temperature fluctuations by sampling from the PDF. From DNS, we use histograms and statistical quantities to obtain the shape of the PDF for the temperature fluctuations. This determines the number of parameters needed to predict the distribution. We analyze the data from the DNS by plotting the parameters that describe the PDF against M_t, Da, $\overline{\Delta h^\circ}$, and K_{eq} evaluated using ensemble-averaged quantities during the simulations. Using the bivariate scatterplots, we find a functional relation for the parameters describing the distribution.

Figure 1 plots the skewness, $S_{T'}$, and flatness, $F_{T'}$, factors for typical reacting simulations. After the initial transient $S_{T'}$ is nearly zero, and $F_{T'}$ is about 3; these values indicate that the temperature fluctuations may be characterized by a Gaussian distribution. Two parameters describe a Gaussian, the mean and the standard deviation. We choose to look for a distribution of the normalized temperature fluctuations, $T'/\langle T\rangle$. In this way, the mean is zero and we only need to predict the standard deviation, which is given by $T'_{\text{RMS}}/\langle T\rangle$. When analyzing the results, we only consider the data after the initial transient, which corresponds to $t/\tau_t > 0.25$.

The scatterplots indicate that $T'_{\text{RMS}}/\langle T\rangle$ changes considerably with Da and M_t during the simulations. K_{eq} is a function of temperature and also affects the standard deviation. Figure 2 shows a functional relation of $T'_{\text{RMS}}/\langle T\rangle$ for the nitrogen dissociation simulations. We observe that when plotting $T'_{\text{RMS}}/\langle T\rangle$ versus the relative heat release times a length ratio, λ/l_E, the data collapses into a power fit. The length ratio is defined from the following relation between the governing parameters:

$$\begin{aligned} \lambda/l_E &= \frac{u'\tau_t}{a\tau_c^*} \\ &= M_t\ Da|\log(K_{eq})|. \end{aligned} \tag{21}$$

$u'\ \tau_t$ is the distance, λ, traveled by a particle of fluid moving at the speed of the turbulent intensity. We have redefined the chemical time scale (20) to take into account the effect of the equilibrium constant, $\tau_c^* = \tau_c|\log(K_{eq})|^{-1}$. Then, $a\ \tau_c^*$ is the distance, l_E, covered

by the acoustic radiation due to temperature fluctuations, and gives the definition of the expansion length, l_E. Moin[24] argues that the chemical process must be independent of the turbulence length scale, since it occurs at a molecular-level. Martín and Candler[11] find that the turbulence-chemistry interaction is independent of the Reynolds number for the range of Re_λ that they consider. Thus, it may be surprising that the length ratio gives a relation for $T'_{\text{RMS}}/\langle T\rangle$. However, the Taylor microscale is defined by the velocity scale of the inertial range eddies and the time scale associated with the dissipative eddies.[25] Therefore, the Taylor microscale is not associated with a particular eddy size. The DNS results show that λ/l_E is always less than 1. As λ/l_E approaches one, $T'_{\text{RMS}}/\langle T\rangle$ is large which indicates a strong turbulence-chemistry interaction. This situation corresponds to the case where the fluid motion covers a similar distance to that covered by the acoustic radiation induced by the temperature fluctuations. However, as λ/l_E approaches zero the thermal expansion outruns the fluid motion and the interaction is weak. This is reflected in the small values of $T'_{\text{RMS}}/\langle T\rangle$. In addition, $T'_{\text{RMS}}/\langle T\rangle$ is affected by the amount of relative heat released to the flow.[11] Thus, the length ratio is modulated by $\overline{\Delta h^\circ}$ to give the relation for the standard deviation:

$$T'_{\text{RMS}}/\langle T\rangle = A(\overline{\Delta h^\circ}\lambda/l_E)^B, \tag{22}$$

where A and B are constants listed in Table I.

While the above relation (22) and physical argument hold for exothermic reactions, the treatment of endothermic reactions must be a different one. When the flow reaches the required internal energy to permit the dissociation of molecules the reactions become endothermic and the flow becomes incompressible.[11] Thus, the magnitude of the temperature fluctuations is reduced by the chemical reactions and the acoustic radiation is nullified. In this situation, the temperature fluctuations are proportional to M_t^2. This is also reflected in Fig. 2, where the filled symbols follow a straight vertical line and correspond to the part of the simulation where the reactions are endothermic. Consider Fig. 3 which plots $T'_{\text{RMS}}/\langle T\rangle$ versus M_t^2 for nitrogen reactions at different initial Mach numbers. The straight line indicates the values of the standard deviation when the chemical reactions are endothermic. And the empty symbols that lie outside the straight line correspond to $T'_{\text{RMS}}/\langle T\rangle$ when the chemical reactions are exothermic. Thus for endothermic reactions the standard deviation is given by:

$$T'_{\text{RMS}}/\langle T\rangle = constant\ M_t^2, \tag{23}$$

where the constant of proportionality is 0.9 for nitrogen dissociation, and 0.48 for oxygen dissociation. Figures 4a and 4b show the curve fits for the oxygen dissociation.

A simple single-variable PDF representation of T' gives no distinction between positive or negative temperature fluctuations. Thus, given the PDF for $T'/\langle T\rangle$, we use a conditional sampling to obtain the temperature fluctuations at each point of the flow. Figure 5 shows scatter plots of the temperature fluctuations against the pressure fluctuations, $P'/\langle P\rangle$ at $t/\tau_t = 0.5$ and 2. We observe that T' is positively correlated with P' for most part of the flow domain during the DNS. In the case of a LES, we can extrapolate the sign of T' using a double filter[14] to obtain the sign of the resolved P'.

Model evaluation

We consider the situation where the resolved-scale temperature is known from the solution of the conservation equations, but the temperature fluctuations are unknown. At every time step during an exothermic simulation, we compute $T'_{\text{RMS}}/\langle T\rangle$ using the corresponding power law in terms of M_t, Da, $\overline{\Delta h^\circ}$, and K_{eq} evaluated using ensemble-averaged quantities. At every point in space, we conditionally sample from the Gaussian PDF described by $T'_{\text{RMS}}/\langle T\rangle$ and zero mean. Based on the new T', we compute the new temperature. This procedure results in a physically correct statistical average of the subgrid-scale temperature fluctuations and the chemical source term. In the following paragraphs we evaluate the model by comparison to the DNS results.

For nitrogen dissociation with initial $M_t = 0.52$ and initial N_2 mass fraction of 0.3 and 0.8, Fig. 6a plots the time evolution of T'_{RMS}. Let us first consider the DNS results. For both simulations the reactions are initially exothermic and the temperature increases. During the simulation with initial N_2 mass fraction of 0.3, the temperature reaches an optimal value for the recombination of nitrogen atoms, and the reaction becomes endothermic near $t/\tau_t = 1$. Thus, T'_{RMS} reaches nearly 325 K in less than 0.25 t/τ_t. But T'_{RMS} decays rapidly during the rest of the simulation, showing weak turbulence-chemistry interaction at later times. In contrast, for the simulation with initial mass fraction of 0.8, the reaction is still exothermic passed $t/\tau_t = 2$. T'_{RMS} reaches roughly 175 K in 0.25 and is maintained during the simulation. Consider now the predictions given by the temperature fluctuation model. For both simulations the model predicts T'_{RMS} accurately. For $\langle c_{N_2}\rangle_\circ = 0.3$ the expression for the standard deviation is switched from (22) to (23) near $t/\tau_t = 0.5$. When $\overline{\Delta h^\circ}\lambda/l_E < M_t$. Figure 6b shows that the model represents c'_{RMS} acceptably during the simulation. It should be noted that the magnitudes of c'_{RMS} given by the DNS are very small. Such small changes in species fluctuations do not contribute significantly to the production of species. And therefore are not important. Figure 6c shows that the model represents $\langle w_{N_2}\rangle$ correctly during the simulation.

To further illustrate the performance of the model, we consider two cases for the dissociation of O_2. Figure 7 plots the modeled and DNS results for simulations with initial $M_t = 0.52$ and initial O_2 mass fraction of 0.3 and 0.8.

For the previous simulations, Fig. 8 plots the correction factor appearing in (18) and given by the DNS. This Fig. shows that the temperature fluctuations contribute significantly to the species production early during the simulations, when the reactions are exothermic. However when the reactions become endothermic, such are the cases with $\langle c_{N_2} \rangle_\circ = \langle c_{O_2} \rangle_\circ = 0.3$, the temperature fluctuations are small and do not contribute to the production of species considerably.

The model also shows good agreement with other turbulent quantities such us ensemble and RMS values of T, w_s, c_s, and turbulent kinetic energy decay. Higher moments such as dilatation values are not well predicted. When the model is turned on, the dilatation values over shoot. This is a direct consequence of the procedure that we use to test the model.

Conclusions

A PDF approach is used to develop a subgrid-scale temperature fluctuation model for the closure of the chemical source term in large-eddy simulations of hypersonic flows. We use a DNS database to obtain the shape of the distribution for $T'/\langle T \rangle$. We find that the distribution is Gaussian and can be described by the standard deviation, $T'_{\text{RMS}}/\langle T \rangle$, and zero mean. For exothermic reactions the magnitude of the temperature fluctuations is enhanced and the standard deviation can be expressed as $A(\overline{\Delta h^\circ}\lambda/l_E)^B$. Where λ/l_E is directly obtained from the non-dimensional governing parameters, and it represents the ratio of the local characteristic distance covered by the fluid motion to the characteristic distance covered by the acoustic radiation. For endothermic reactions, the flow becomes more incompressible and the temperature fluctuations scale with M_t^2. We find that T' is positively correlated with P' for most part of the flow domain. We use this condition to obtain the sign of the modeled temperature fluctuations. We evaluate the model by comparison to DNS and find good agreement of results. Previous results[11] indicate that the chemistry-turbulence interaction is independent of the turbulent length scales. Thus, we expect the constants appearing in (22) and (23) to be independent of the grid size filter.

In the context of a hypersonic boundary layer, the values of the governing parameters and therefore the length ratio can be obtained by averaging along path lines or planes parallel to the wall. Then, the temperature fluctuations may be obtained by conditionally sampling from the probability density function described by the calibrated power curves

for exothermic reactions. For endothermic reactions, the magnitude of the temperature fluctuations is small, and will not contribute significantly to the production of species. Therefore, the temperature fluctuations may not need modeling in a situation where the reactions are endothermic. It still remains to be determined if a Gaussian probability density function can be used to accurately represent the temperature fluctuations in a boundary layer. Owen et al.[26] find that for a cold wall boundary layer at $M_\infty = 7$ the probability density function for the temperature fluctuations is skewed near the wall.

Acknowledgments

We would like to acknowledge support from the Air Force Office of Scientific Research Grant number AF/F49620-96-1-0269. A portion of the computer time was provided by the University of Minnesota Supercomputing Institute.

References

[1]S.S. Girimaji, "Assumed β-pdf model for turbulent mixing: validation and extension to multiple scalar mixing," Combust. Sci. Tech. **78**, 177 (1991).

[2]F. Gao, and E.E. O'Brien, "Direct numerical simulations of reacting flows in homogeneous turbulence," AIChE J. **37**, 1459 (1991).

[3]R.L. Gaffney, J.A. White and J.P. Drummond, "Modeling turbulence/chemistry interactions using assumed PDF methods," AIAA Paper No. 92-3638 (1992).

[4]S.H. Frankel, V. Adumitroaie, C.K. Madnia and P. Givi, "Large eddy simulation of turbulent reacting flows by assumed PDF methods," FED-Engineering Applications of Large Eddy Simulations ASME **162**, 81 (1993).

[5]A.W. Cook and J.J. Riley, "A subgrid model for equilibrium chemistry in turbulent flows," Phys. Fluids **6**, 2868 (1994).

[6]C. Dopazo and L. Valiño, "PDF approach and stochastic models of the turbulent mixing of inert and reactive statistically homogeneous scalar fields," Transp. Theor. Statist. Phys. **23**, 339 (1994).

[7]P. Givi, V. Adumitronie, G.J. Sabini and G.S. Shieh, "LES, DNS and RANS for the analysis of high-speed turbulent reacting flows," NASA-CR-196822 (1994).

[8]R.L. Gaffney, J.A. White, S.S. Girimaji and J.P. Drummond, "Modeling temperature and species fluctuations in turbulent, reacting flows," Comput. Syst. Eng. **5**, 117 (1994).

[9]A.W. Cook, J.J. Riley, and G. Kosàly, "A laminar flamelet approach to subgrid-scale chemistry in turbulent flows," Combust. Flame **109**, 332 (1997).

[10]P.A. Nooren, H.A. Wouters, T.W.J. Peeters, D. Roekaerts, "Monte Carlo PDF modelling of a turbulent natural-gas diffusion flame," U. Maas, and D. Schmidt, Combust. Theor. Modelling **1**, 79 (1997).

[11]M.P. Martín and G.V. Candler, "Effect of chemical reactions on the decay of isotropic homogeneous turbulence," AIAA Paper No. 96-2060 (1996).

[12]R.N. Gupta, J.M., Yos, R.A., Thompson, and K. Lee, "A review of reaction rates and thermodynamic and transport properties for an 11-species air model for chemical and thermal non-equilibrium calculations to 30,000 K," NASA Reference Publication 1232 (1990).

[13]C. Park, "On the convergence of computation of chemically reacting flows," AIAA Paper No. 85-0247 (1985).

[14]Germano, M. , U. Piomelli, P. Moin, and W.H. Cabot, "A dynamic subgrid-scale eddy viscosity model," Phys. Fluids **3**, 1760 (1991).

[15]Lilly, D.K. , "A proposed modification of the Germano subgrid-scale closure method," Phys. Fluids **4**, 633 (1992).

[16]Moin, P. , K. Squires, W. Cabot, and S. Lee, "A dynamic subgrid-scale model for compressible turbulence and scalar transport," Phys. Fluids **3**, 2746 (1991).

[17]Spyropoulos, E.T. , G.A. Blaisdell, "Evaluation of the dynamic model for simulations of compressible decaying isotropic turbulence," AIAA J. **34**, 990 (1996).

[18]Ghosal, S., T.S. Lund, P. Moin, and K. Akselvoll, "A dynamic localization model for large-eddy simulation of turbulent flows," J. Fluid Mech., **286**, 229 (1995).

[19]Gao, F., and E.E. O'Brien, "A large-eddy simulation scheme for turbulent reacting flows," Phys. Fluids **5**, 1282 (1993).

[20]Réveillon, J., and L. Vervisch, "Response of the dynamic LES model to heat release induced effects," Phys. Fluids **8**, 2248 (1996).

[21]Lele, S.K., "Compact finite difference scheme with spectral-like resolution," J. Comp. Phys. **103**, 16 (1992).

[22]J.R. Ristorcelli and G.A. Blaisdell, "Consistent initial conditions for the DNS of compressible turbulence," Phys. Fluids **9**, 4 (1997).

[23]S.B. Pope, "PDF methods for turbulent reactive flows," Prog. Energy and Combust. Sci. **11**, 119 (1985).

[24]P. Moin, "Progress in large eddy simulation of turbulent flows," AIAA Paper No. 97-0749 (1997).

[25]H. Tennekes and J.L. Lumley, *A first course in turbulence* (MIT Press, Cambridge, 1972), Chap. 3.

[26]F.K. Owen, C.C. Horstman, and M.I. Kussoy, "Mean and fluctuating flow measurements of a fully-developed, non-adiabatic, hypersonic boundary layer ," J. Fluid Mech. **70**, 393 (1975).

Table Captions

TABLE I. List of constants for $T'_{\mathrm{RMS}}/\langle T\rangle = \mathrm{A}\left(\overline{\Delta h^{\circ}}\ \lambda/l_E\right)^{\mathrm{B}}$.

TABLE I

	N_2		O_2	
M_t	A	B	A	B
0.35	0.016	0.199	0.062	0.179
0.52	0.043	0.225	0.048	0.306

Figure Captions

FIGURE 1. Time evolution of temperature fluctuations skewness, $S_{T'}$, and flatness, $F_{T'}$, factors for N_2 dissociation at initial $M_t = 0.52$.

FIGURE 2. Standard deviation versus the modulated length ratio, $\overline{\Delta h^\circ}\lambda/l_E$, for N_2 dissociation at initial $M_t = 0.35, 0.52$.

FIGURE 3. Standard deviation versus M_t^2 for N_2 dissociation at initial $M_t = 0.17, 0.35$ and, 0.52.

FIGURE 4. Standard deviation for O_2 dissociation (a) versus the modulated length ratio, $\overline{\Delta h^\circ}\lambda/l_E$, at initial $M_t = 0.35, 0.52$; and (b) versus M_t^2 at initial $M_t = 0.17, 0.35$ and, 0.52.

FIGURE 5. Scatter plot of the normalized temperature fluctuations, $T'/\langle T\rangle$, and the normalized pressure fluctuations, $P'/\langle P\rangle$, for N_2 dissociation at initial $M_t = 0.52$, and $\langle c_{N_2}\rangle_\circ = 0.8$, after (a) $t/\tau_t = 0.5$; and (b) $t/\tau_t = 2$.

FIGURE 6. Model performance for N_2 dissociation at initial $M_t = 0.52$ and $\langle c_{N_2}\rangle_\circ$ =0.3, 0.8. Time evolutions of (a) RMS temperature fluctuation; (b) RMS of species fluctuations; and (c) ensemble average of the source term, $\langle w_{N_2}\rangle/\langle w_{N_2}\rangle_\circ$.

FIGURE 7. Model performance for O_2 dissociation at initial $M_t = 0.52$ and $\langle c_{O_2}\rangle_\circ$ =0.3, 0.8. Time evolutions of (a) RMS temperature fluctuation; and (b) ensemble average of the source term, $\langle w_{O_2}\rangle/\langle w_{O_2}\rangle_\circ$.

FIGURE 8. Time evolution of factor $\left(\frac{\theta}{\langle T\rangle} + \eta\right)\frac{T'}{\langle T\rangle}$ appearing in (18) for N_2 dissociation with (a) $\langle c_{N_2}\rangle_\circ = 0.3$, solid; (b) $\langle c_{N_2}\rangle_\circ = 0.8$, dashed; and for O_2 dissociation with (c) $\langle c_{O_2}\rangle_\circ = 0.3$, long-dashed; and (d) $\langle c_{O_2}\rangle_\circ = 0.8$, dashed-double dotted; all simulations start with initial $M_t = 0.52$.

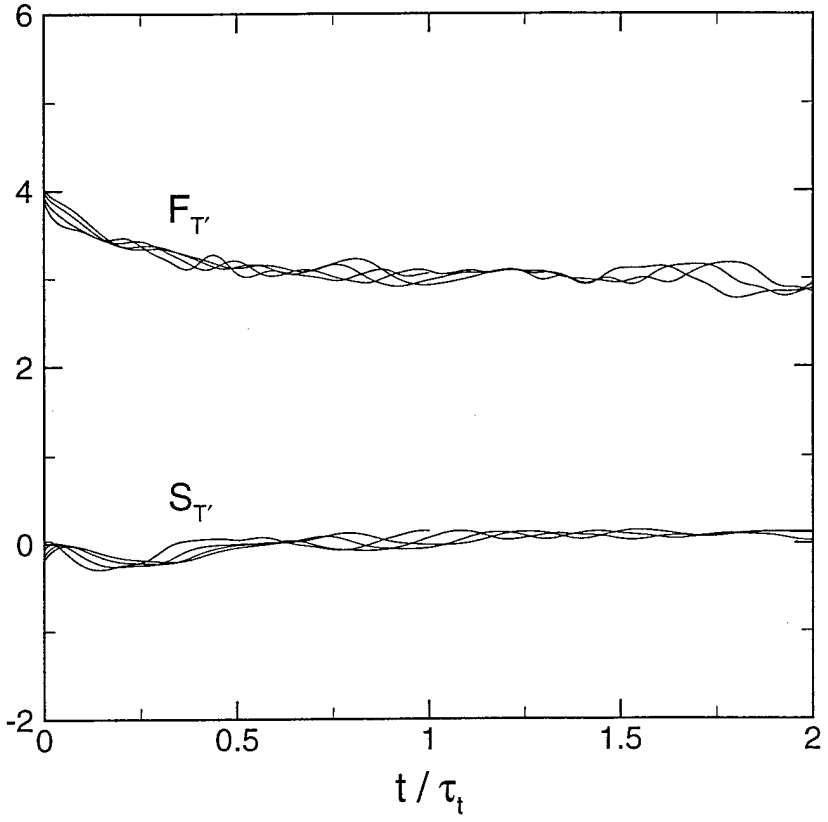

FIG. 1)

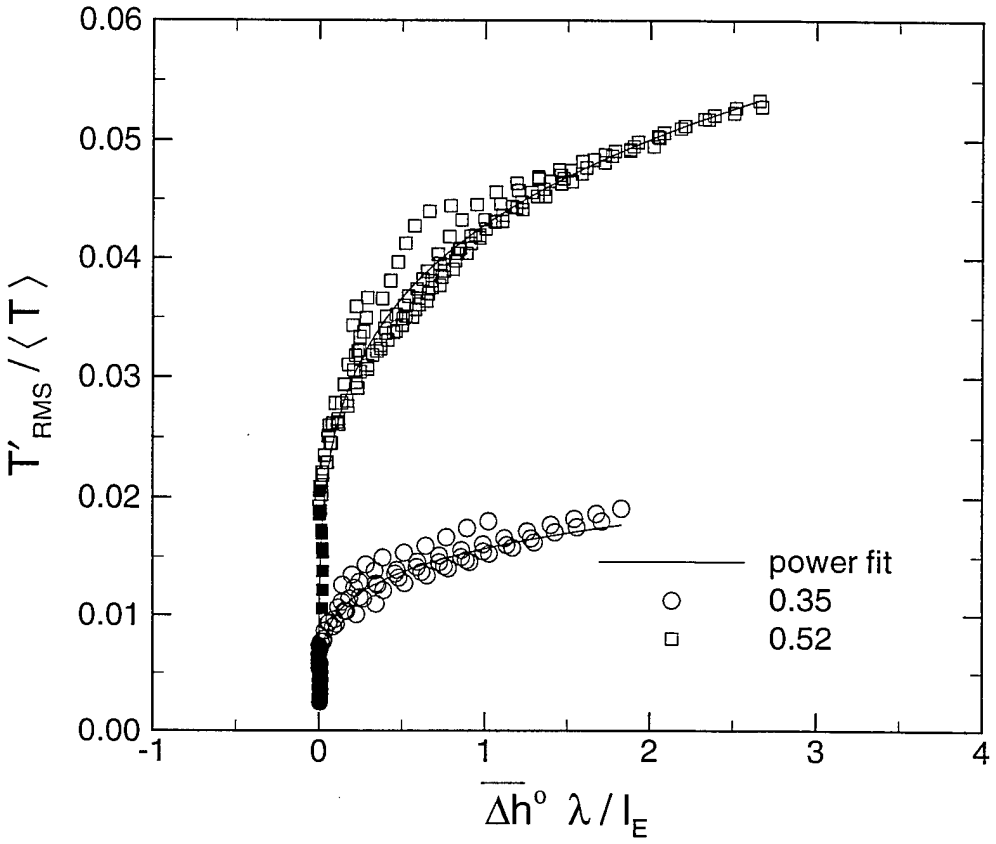
0.06
0.05
0.04
0.03
0.02
0.01
0.00
-1
0
1
2
3
4
T'RMS / ⟨ T ⟩
Δh° λ / lE
power fit
0.35
0.52

FIG. 2)

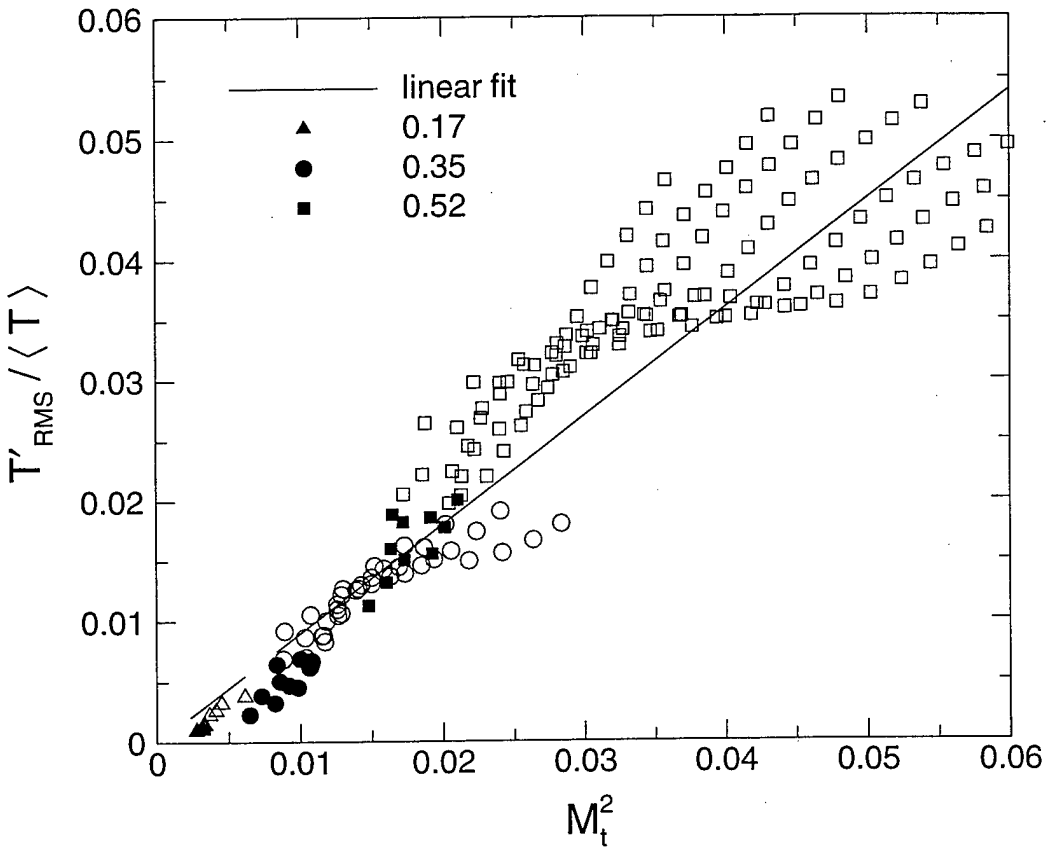
linear fit
0.17
0.35
0.52
0.06
0.05
0.04
0.03
0.02
0.01
0
0
0.01
0.02
0.03
0.04
0.05
0.06
T'RMS / ⟨ T ⟩
M2t

FIG. 3)

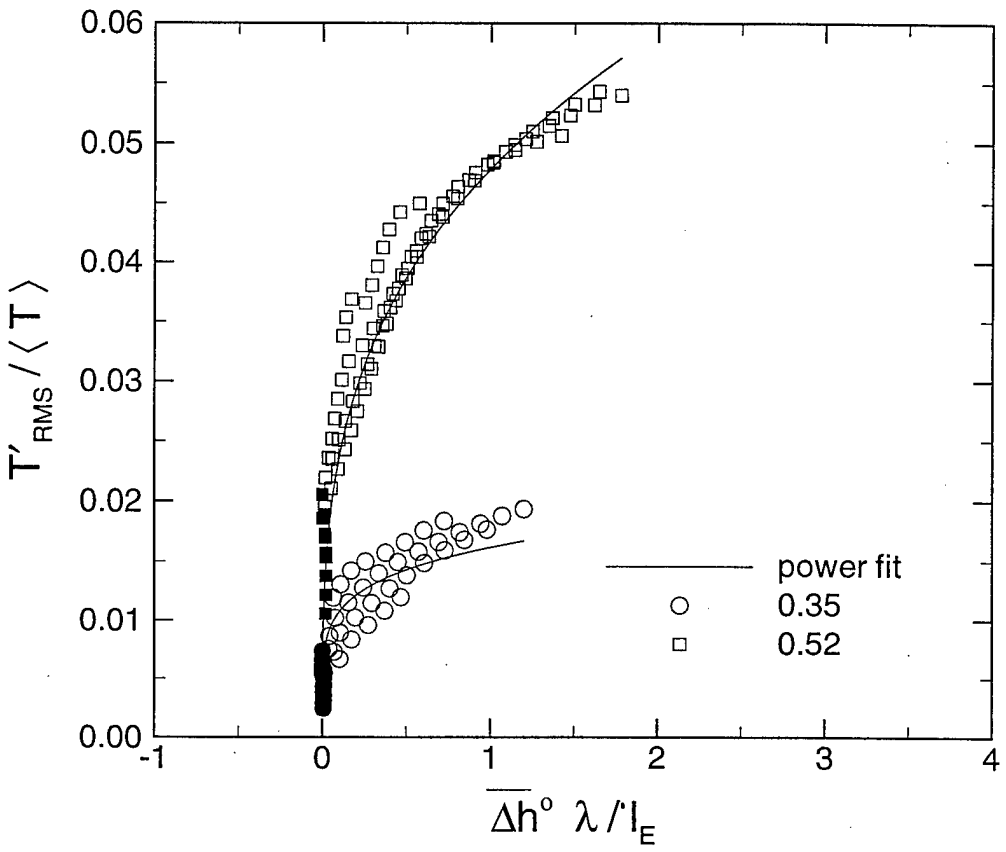
0.06
0.05
0.04
0.03
0.02
0.01
0.00
-1
0
1
2
3
4
T'RMS / ⟨ T ⟩
Δh° λ /'lE
power fit
0.35
0.52

FIG. 4 a)

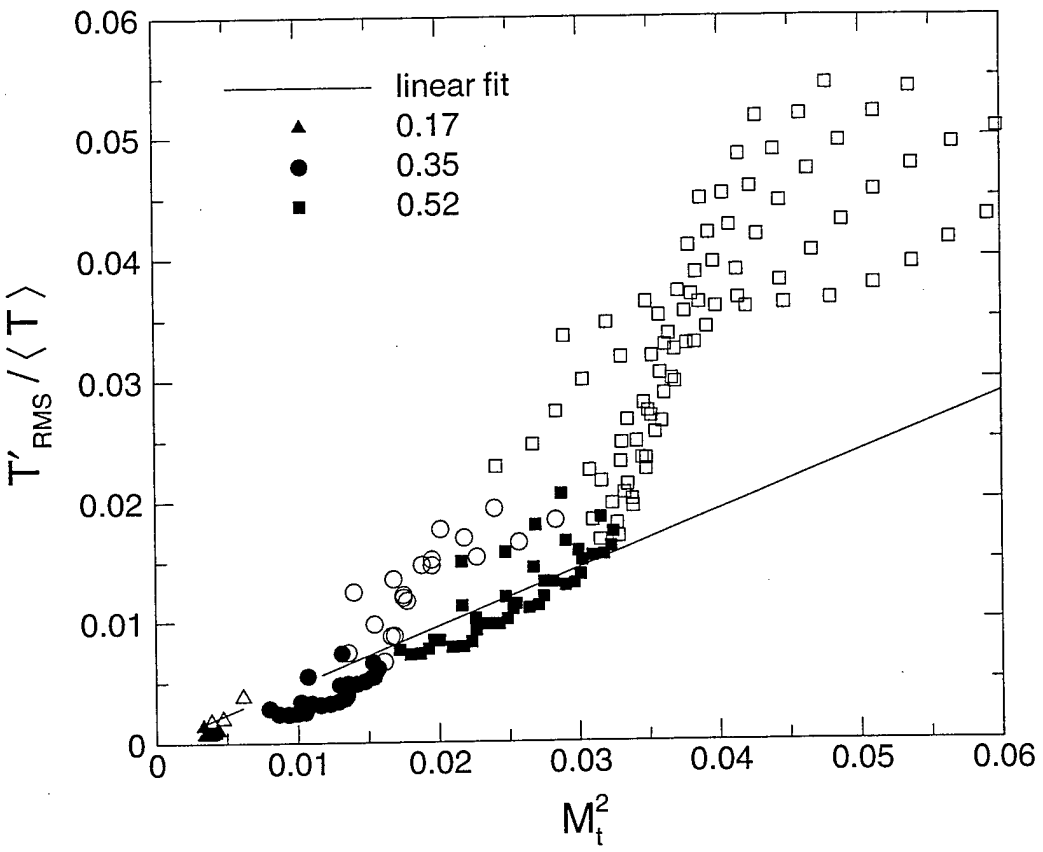
linear fit
0.17
0.35
0.52
0.06
0.05
0.04
0.03
0.02
0.01
0
0
0.01
0.02
0.03
0.04
0.05
0.06
T'RMS / ⟨ T ⟩
M2t

FIG. 4 b)

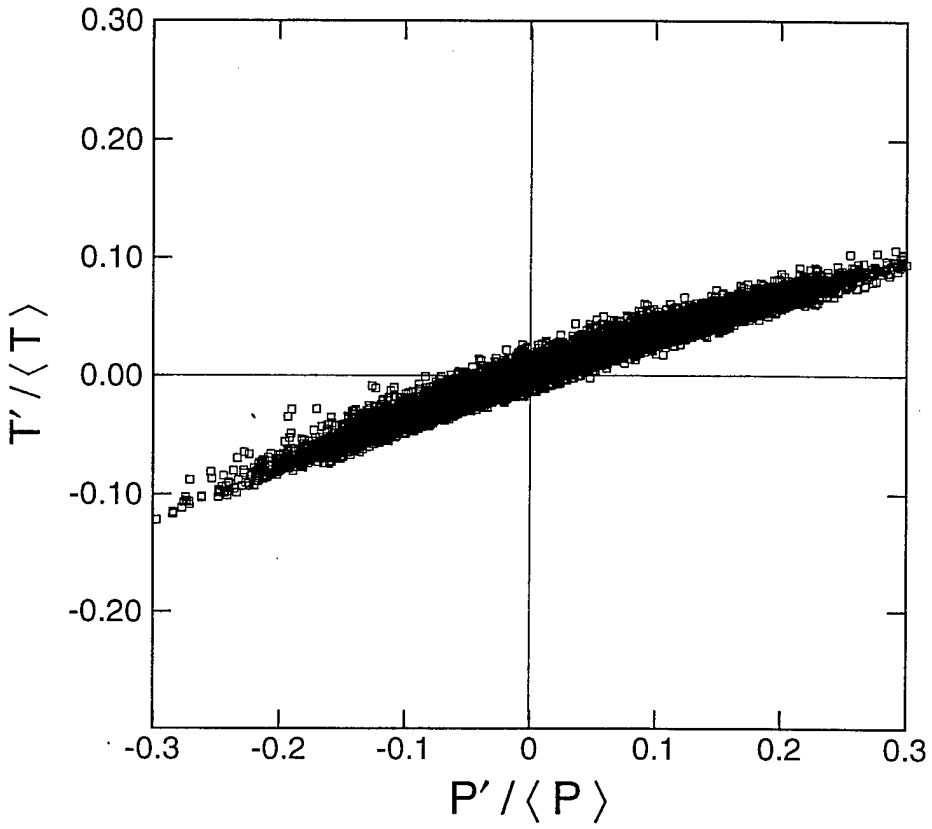

FIG. 5 a)

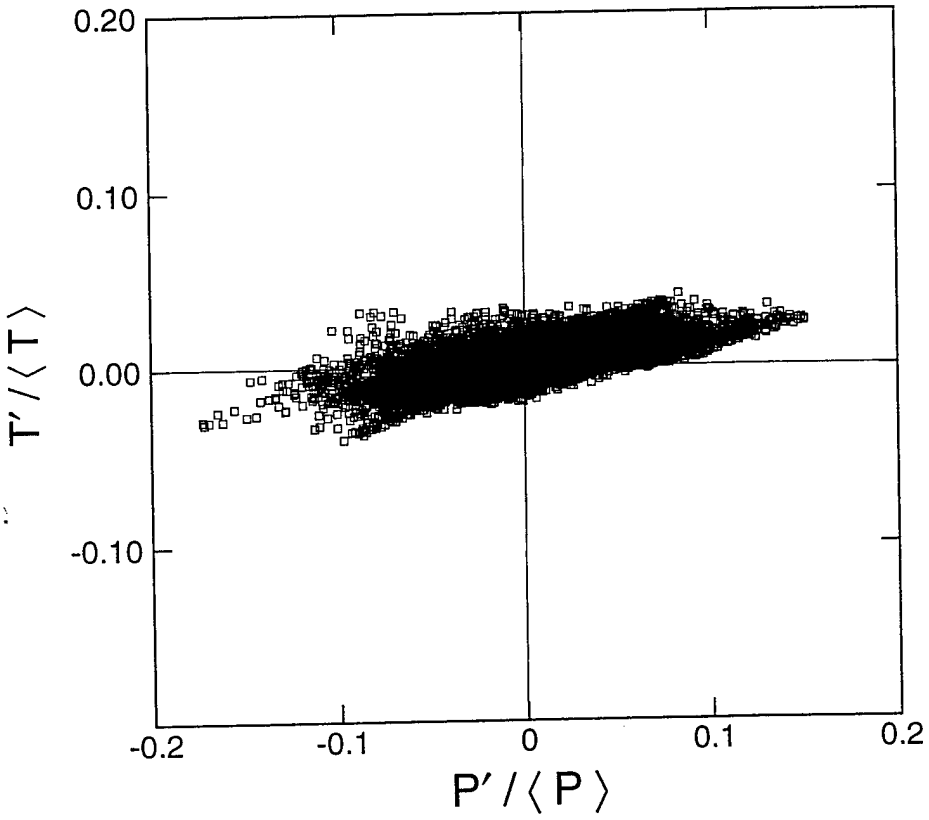

FIG. 5 b)

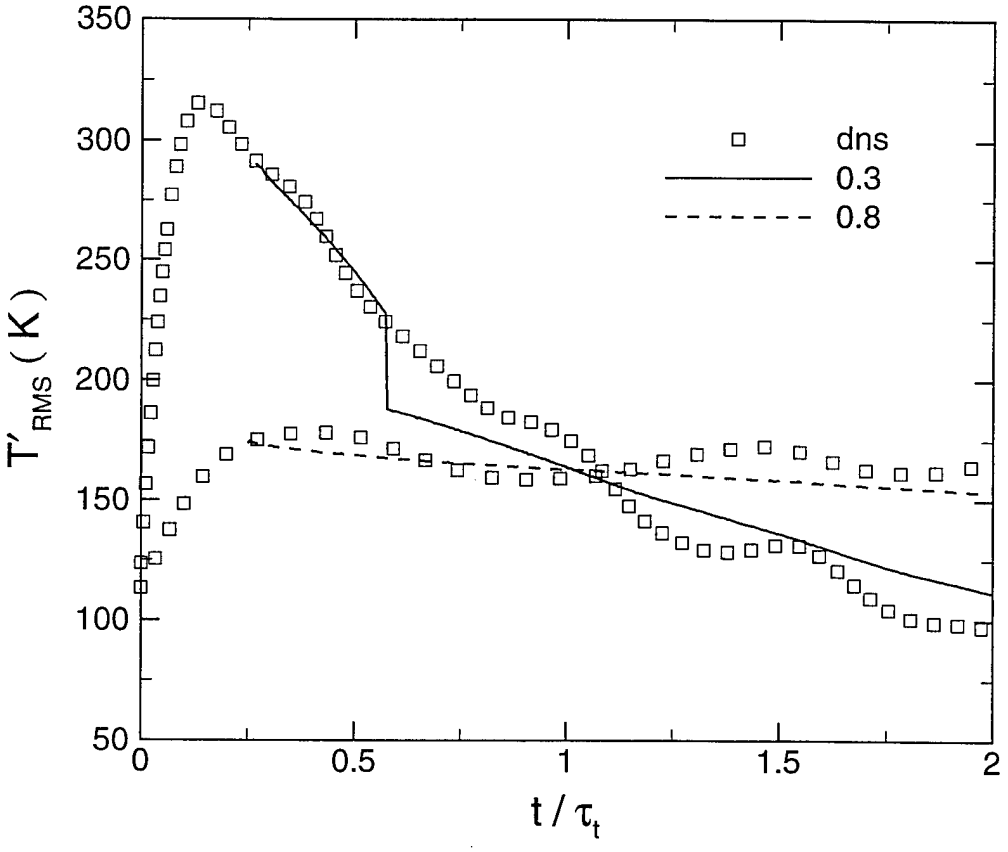

FIG. 6 a)

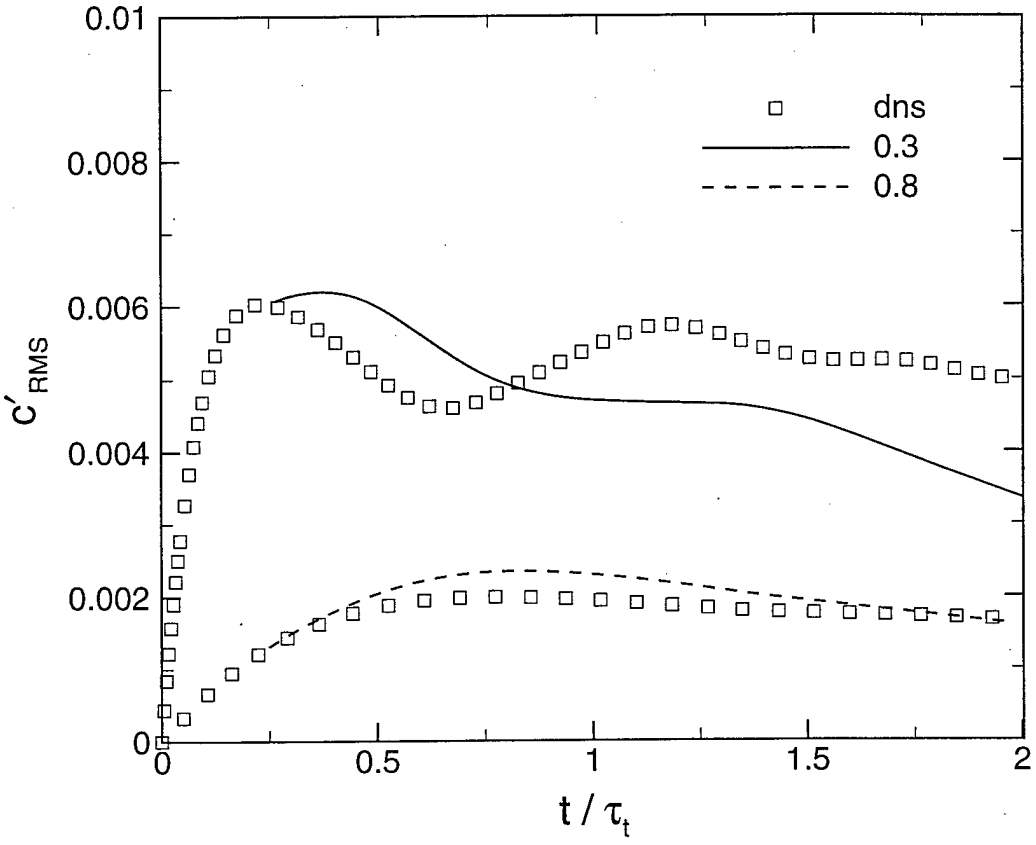

FIG. 6 b)

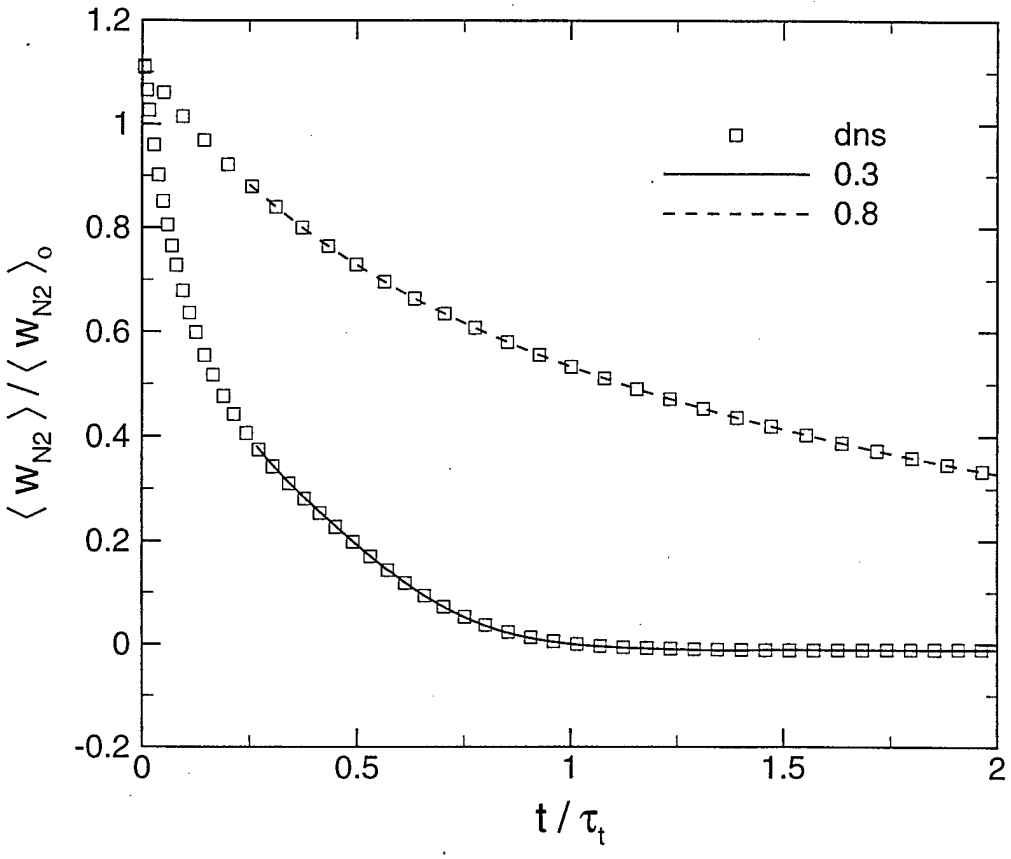

FIG. 6 c)

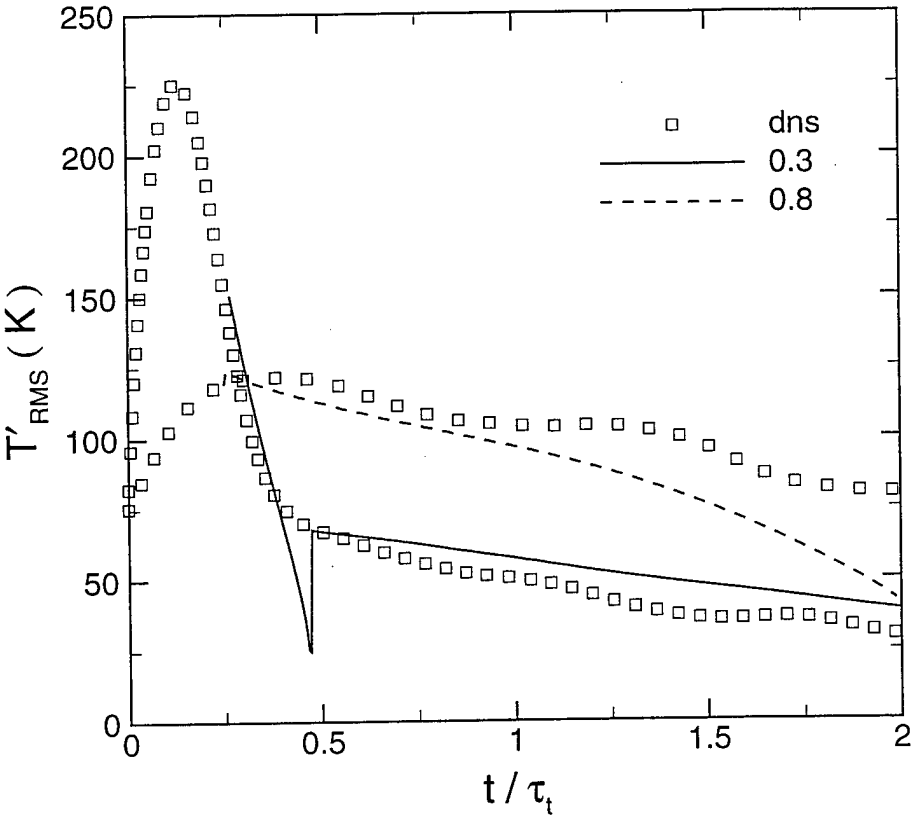

FIG. 7 a)

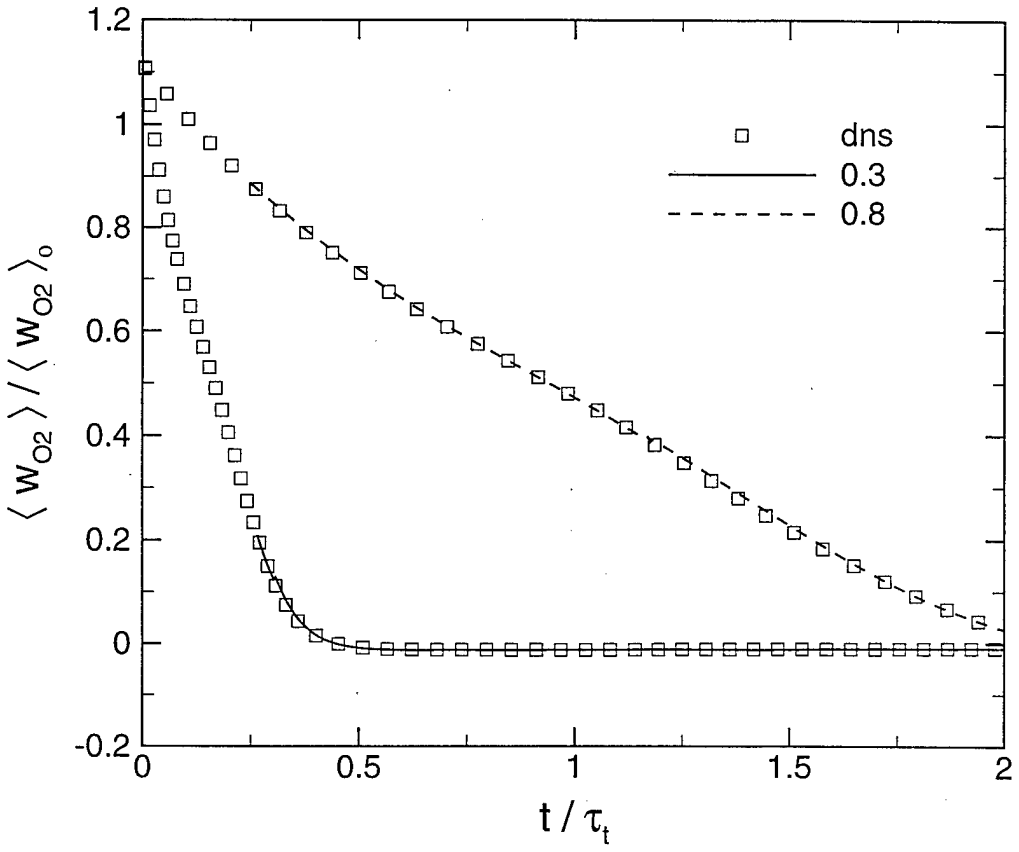
1.2
1
0.8
0.6
0.4
0.2
0
-0.2
0
0.5
1
1.5
2
$\langle W_{O2} \rangle / \langle W_{O2} \rangle_o$
t / τ_t
dns
0.3
0.8

FIG. 7 b)

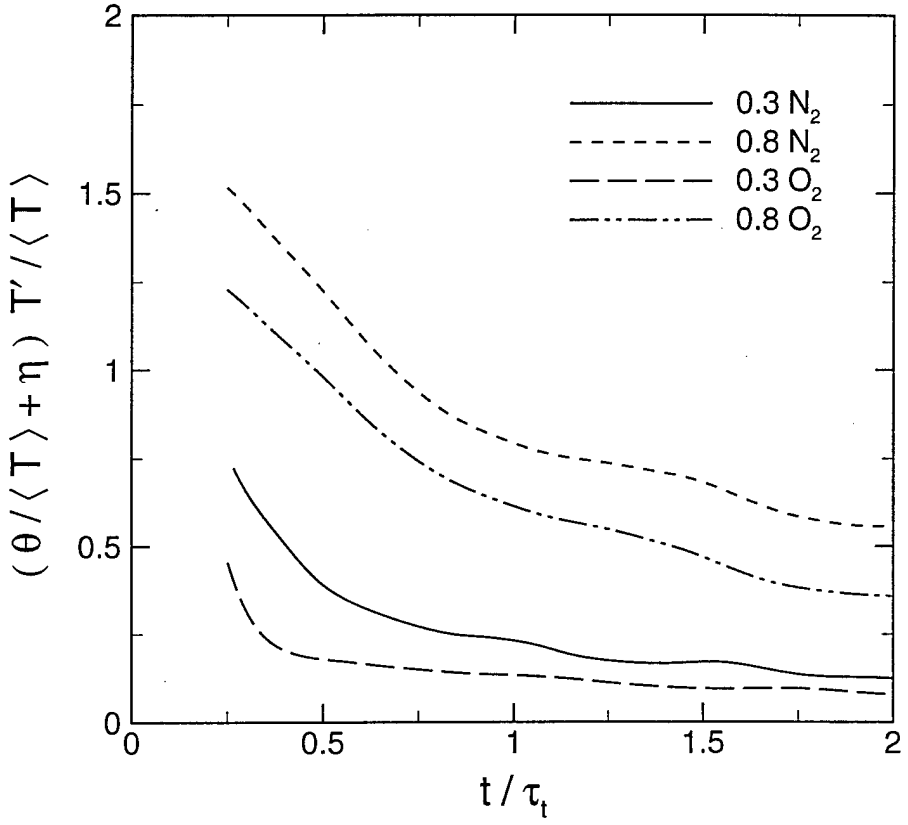
2
1.5
1
0.5
0
0
0.5
1
1.5
2
$(\theta/\langle T\rangle+\eta)\ T'/\langle T\rangle$
t/τ_t
0.3 N_2
0.8 N_2
0.3 O_2
0.8 O_2

FIG. 8)